



**HAL**  
open science

## Product Detection of the CH Radical Reactions with Ammonia and Methyl-Substituted Amines

Jérémy Bourgalais, Kacee L. Caster, Olivier Durif, David L. Osborn,  
Sébastien D. Le Picard, Fabien Goulay

► **To cite this version:**

Jérémy Bourgalais, Kacee L. Caster, Olivier Durif, David L. Osborn, Sébastien D. Le Picard, et al.. Product Detection of the CH Radical Reactions with Ammonia and Methyl-Substituted Amines. *Journal of Physical Chemistry A*, 2019, 123 (11), pp.2178-2193. 10.1021/acs.jpca.8b11688 . hal-02089225

**HAL Id: hal-02089225**

**<https://univ-rennes.hal.science/hal-02089225>**

Submitted on 11 Apr 2019

**HAL** is a multi-disciplinary open access archive for the deposit and dissemination of scientific research documents, whether they are published or not. The documents may come from teaching and research institutions in France or abroad, or from public or private research centers.

L'archive ouverte pluridisciplinaire **HAL**, est destinée au dépôt et à la diffusion de documents scientifiques de niveau recherche, publiés ou non, émanant des établissements d'enseignement et de recherche français ou étrangers, des laboratoires publics ou privés.

1  
2  
3 **Product Detection of the CH Radical Reactions with Ammonia and**  
4  
5  
6 **Methyl-Substituted Amines**  
7

8 Jeremy Bourgalais,<sup>1</sup> Kacee L. Caster,<sup>2</sup> Olivier Durif,<sup>3</sup> David L. Osborn,<sup>4</sup> Sebastien D. Le  
9 Picard,<sup>3</sup> and Fabien Goulay<sup>2,\*</sup>  
10

11  
12  
13 <sup>1</sup> *LATMOS/IPSL, UVSQ Université Paris-Saclay, Sorbonne Université, CNRS, Guyancourt,*  
14  
15 *France*  
16

17  
18 <sup>2</sup> *Department of Chemistry, West Virginia University, Morgantown, West Virginia 26506, USA*  
19

20  
21 <sup>3</sup> *Astrophysique de Laboratoire, Univ Rennes, CNRS, IPR (Institut de Physique de Rennes) -*  
22 *UMR 6251, F-35000 Rennes, France*  
23

24  
25 <sup>4</sup> *Combustion Research Facility, Mail Stop 9055, Sandia National Laboratories, Livermore,*  
26  
27 *California 94551, USA*  
28

29 **\*Corresponding Author:** [Fabien.Goulay@mail.wvu.edu](mailto:Fabien.Goulay@mail.wvu.edu)  
30  
31  
32  
33  
34  
35  
36  
37  
38  
39  
40  
41  
42  
43  
44  
45  
46  
47  
48  
49  
50  
51  
52  
53  
54  
55  
56  
57  
58  
59  
60

1  
2  
3  
4  
5  
6  
7  
8  
9  
10  
11  
12  
13  
14  
15  
16  
17  
18  
19  
20  
21  
22  
23  
24  
25  
26  
27  
28  
29  
30  
31  
32  
33  
34  
35  
36  
37  
38  
39  
40  
41  
42  
43  
44  
45  
46  
47  
48  
49  
50  
51  
52  
53  
54  
55  
56  
57  
58  
59  
60  
**ABSTRACT**

Reactions of the methylidyne (CH) radical with ammonia (NH<sub>3</sub>), methylamine (CH<sub>3</sub>NH<sub>2</sub>), dimethylamine ((CH<sub>3</sub>)<sub>2</sub>NH), and trimethylamine ((CH<sub>3</sub>)<sub>3</sub>N), have been investigated under multiple collision conditions at 373 K and 4 Torr. The reaction products are detected using soft photoionization coupled to orthogonal acceleration time-of-flight mass spectrometry at the Advanced Light Source (ALS) synchrotron. Kinetic traces are employed to discriminate between CH reaction products and products from secondary or slower reactions. Branching ratios for isomers produced at a given mass and formed by a single reaction are obtained by fitting the observed photoionization spectra to linear combinations of pure compound spectra. The reaction of the CH radical with ammonia is found to form mainly imine, HN=CH<sub>2</sub>, in line with an addition–elimination mechanism. The singly methyl substituted imine is detected for the CH reactions with methylamine, dimethylamine, and trimethylamine. Dimethylimine isomers are formed by the reaction of CH with dimethylamine, while trimethylimine is formed by the CH reaction with trimethylamine. Overall, the temporal profiles of the products are not consistent with the formation of amino carbene products in the reaction flow tube. In the case of the reactions with methylamine and dimethylamine, product formation is assigned to an addition-elimination mechanism similar to that proposed for the CH reaction with ammonia. However, this mechanism cannot explain the products detected by the reaction with trimethylamine. A C–H insertion pathway may become more probable as the number of methyl group increases.

## 1. INTRODUCTION

Ammonia and its amine derivatives are emitted as gases in the atmosphere from a variety of sources such as biomass burning, vegetation, combustion, as well as industry.<sup>1,2</sup> These nitrogen-containing molecules are of special interest in combustion environments where they impact the oxidation and ignition of hydrocarbon fuels.<sup>3,4</sup> In addition, their chemistry in reactive carbon-rich environments may play a significant role in the formation of NO<sub>x</sub>.<sup>5-10</sup> An improved utilization of biomass-derived nitrogen-containing compounds as fuels and a better understanding of the role of amines in combustion both require a systematic study of the chemistry of ammonia and substituted amines with combustion relevant radicals.

A large number of experiments have been performed to investigate the reaction of ammonia with radicals such as OH, CN, C<sub>2</sub>H, and CH.<sup>11-15</sup> Although its reaction with the OH radical is found to be slow ( $<5 \times 10^{-13} \text{ cm}^3 \text{ s}^{-1}$  from 230 K to 450 K),<sup>11</sup> ammonia reacts at a significant fraction of the collision rate with the CN,<sup>12</sup> C<sub>2</sub>H,<sup>13</sup> and CH radicals.<sup>14</sup> In the case of the reactions with OH and CN, the products are predicted to mostly be NH<sub>2</sub> + H<sub>2</sub>O and NH<sub>2</sub> + HCN.<sup>13,16,17</sup> The reaction with OH proceeds directly through a HO–H–NH<sub>2</sub> abstraction saddle point,<sup>16</sup> while the reaction with CN initially forms a NC–NH<sub>3</sub> adduct that may rearrange and dissociate to form the final products.<sup>13,17</sup> The most exhaustive experimental and theoretical studies have been performed for the CH + NH<sub>3</sub> reaction.<sup>15</sup> The mechanism has been assigned as addition–elimination, as further described in this introduction. Kinetic investigations with methyl-substituted amines are scarcer and data are available only for reactions with OH and CH radicals.<sup>14,18-22</sup> Reactions with the OH radical proceed with a rate coefficient on the order of  $1 \times 10^{-11} \text{ cm}^3 \text{ s}^{-1}$  and are predicted to occur through interaction of the OH radical with an H-atom of both the amine and methyl groups to give the abstraction products.<sup>18</sup> Reactions of the CH radical with methyl substituted amines are fast ( $>1 \times 10^{-10} \text{ cm}^3 \text{ s}^{-1}$ )<sup>14</sup> although no mechanistic information is available.

1  
2  
3 The methylidyne (CH) radical is an important reactive intermediate detected in  
4 hydrocarbon flames (*e.g.*, methane, acetylene, ethene, ethane, propene, propane).<sup>13,16,23,24</sup> Its  
5 barrier-less addition toward a large number of organic and inorganic functional groups is due  
6 to the carbon atom having both one singly occupied and one empty non-bonding molecular  
7 orbital. Its formation in flames, along with other fuel-derived C<sub>1</sub>-radicals (*e.g.*, CH<sub>3</sub>, CH<sub>2</sub> and  
8 C), occurs primarily from oxidation of small hydrocarbon compounds (*e.g.*, methane,  
9 acetylene).<sup>17,25</sup> Once formed, the CH radical is likely to play a role in the formation of soot  
10 precursors through generation of small cyclic hydrocarbons.<sup>23-28</sup> A major interest of the CH  
11 radical in combustion is its ability to react with molecular nitrogen to form NCN, which is the  
12 dominant source of prompt NO formation in turbulent diffusion flames.<sup>17,25-38</sup> Its reaction with  
13 ammonia is also included in a recent combustion model.<sup>25</sup> As fuel complexity is increased,  
14 there is a need for additional data about the reaction of the CH radical with nitrogen containing  
15 hydrocarbons.

16  
17  
18  
19  
20  
21  
22  
23  
24  
25  
26  
27  
28  
29  
30  
31  
32  
33 Zabarnick *et al.*<sup>14</sup> performed the first kinetic measurements of CH radical reactions with  
34 ammonia and methyl substituted amines. They employed pulsed laser photolysis (PLP) and  
35 laser-induced fluorescence (LIF) to measure rate constants for CH with NH<sub>3</sub>, CH<sub>3</sub>NH<sub>2</sub>,  
36 (CH<sub>3</sub>)<sub>2</sub>NH and (CH<sub>3</sub>)<sub>3</sub>N at temperatures ranging from room temperature up to 677 K. Based on  
37 the observed large rate coefficients they suggested an insertion–elimination mechanism of CH  
38 into one of the N-H bonds followed by rapid dissociation of the energized complex. Bocherel  
39 *et al.*<sup>39</sup> measured the CH + NH<sub>3</sub> reaction also using a PLP–LIF technique in a supersonic flow  
40 reactor between 23 and 295 K. The reaction rate coefficient is 1.37×10<sup>-10</sup> cm<sup>3</sup> s<sup>-1</sup> at 295 K and  
41 displays no significant temperature (2.21×10<sup>-10</sup> cm<sup>3</sup> s<sup>-1</sup> at 23 K) or pressure dependences in  
42 agreement with the study of Zabarnick *et al.*<sup>14</sup> More recently Blitz *et al.*<sup>15</sup> investigated the  
43 products of the CH + NH<sub>3</sub> reaction by measuring the H-atom branching ratio using LIF. The  
44 close to unity H-atom branching ratio combined with high-level (MCSCF/CASSCF)  
45  
46  
47  
48  
49  
50  
51  
52  
53  
54  
55  
56  
57  
58  
59  
60

1  
2  
3 calculations<sup>15</sup> support an insertion–elimination mechanism similar to that proposed for the  
4  
5 reactions of CH with saturated hydrocarbons.<sup>40</sup> In the case of ammonia the insertion is found  
6  
7 to proceed first through the formation of a dative bond<sup>15</sup> between the carbon and the nitrogen  
8  
9 atoms.<sup>15</sup>  
10

11  
12 The aim of the present study is to obtain a general mechanism for the reaction of CH  
13  
14 with amines. For this purpose we present a systematic investigation of the products formed by  
15  
16 reactions of ground state methylidyne CH( $X^2\Pi$ ) radicals with NH<sub>3</sub> and three methyl  
17  
18 derivatives: methylamine (MA) CH<sub>3</sub>NH<sub>2</sub>, dimethylamine (DA) (CH<sub>3</sub>)<sub>2</sub>NH, and trimethylamine  
19  
20 (TA) (CH<sub>3</sub>)<sub>3</sub>N. To probe the reaction products, experiments are performed in a flow reactor  
21  
22 under thermal conditions (373 K and 4 Torr) at the Advanced Light Source (ALS) synchrotron  
23  
24 of Lawrence Berkeley National Laboratory (LBNL). Products sampled from the flow are  
25  
26 detected using tunable vacuum ultraviolet (VUV) photoionization and time-of-flight mass  
27  
28 spectrometry. Kinetic traces and photoionization spectra supported by thermodynamic and  
29  
30 Franck–Condon factor calculations of the species have been used to infer the primary products  
31  
32 of the reactions.  
33  
34  
35  
36

## 37 38 **2. EXPERIMENTAL PROCEDURE**

39  
40 The experiments are performed in a slow flow reactor coupled to a tunable VUV  
41  
42 photoionization orthogonal acceleration time-of-flight mass spectrometer. A detailed  
43  
44 description of the apparatus has been given in the literature<sup>41-43</sup> and only a brief description is  
45  
46 given here. The reactions take place in a flow tube at 373 K and at a pressure of 4 Torr (total  
47  
48 density  $\sim 10^{17}$  cm<sup>-3</sup>). The 100 sccm gas flow consists of a large excess of He with 10% nitrogen  
49  
50 and small amounts of CH-radical precursor (bromoform) and reagent gases (ammonia, MA,  
51  
52 DMA, or TMA) with typical densities of  $\sim 10^{13}$  cm<sup>-3</sup> and  $\sim 10^{14}$  cm<sup>-3</sup> respectively. The  
53  
54 bromoform (CHBr<sub>3</sub>) is placed in a glass vessel and its vapor carried into the main carrier gas  
55  
56 flow by bubbling a controlled flow of He through the liquid. The purities of gases are:  
57  
58  
59  
60

1  
2  
3 bromoform (99%),  $\text{CDBr}_3$  ( $\geq 99\%$ ,  $\geq 99.5$  atom % D),  $\text{NH}_3$  ( $\geq 99.9\%$ ),  $\text{CH}_3\text{NH}_2$  ( $\geq 99\%$ ),  
4  
5  
6  $(\text{CH}_3)_2\text{NH}$  ( $\geq 99\%$ ),  $(\text{CH}_3)_3\text{N}$  ( $\geq 99\%$ ).  
7

8 CH radicals are generated by excimer laser photolysis at 248 nm with a 4 Hz repetition  
9  
10 rate. The laser power output is typically 266 mJ per pulse for a 20 ns pulse duration, with a  
11  
12 photolysis fluence inside the flow tube of  $\sim 20\text{--}50$   $\text{mJ cm}^{-2}$ . Photodissociation occurs via  
13  
14 successive absorption of photons eliminating multiple halogen atoms leading to CH number  
15  
16 density of about  $2.5 \times 10^{10}$   $\text{cm}^{-3}$  in the reaction flow.<sup>44,45</sup>  
17  
18  
19

20 The gas mixture is sampled through a pinhole halfway down the flow tube into a high-  
21  
22 vacuum chamber. A skimmer generates a molecular beam into the ionization chamber where  
23  
24 species are ionized by the quasi-continuous tunable VUV synchrotron radiation of the ALS.  
25  
26 The formed ions are detected through time-of-flight mass spectrometry by recording their  
27  
28 arrival time with respect to the extraction pulse and laser pulse. The setup leads to complete  
29  
30 time- and energy-resolved mass spectra by averaging 200-500 laser pulses for each ionizing  
31  
32 photon energy. The photoionization spectra are obtained from three independent data sets,  
33  
34 averaged and integrated, over the mass-to-charge ratio and time window of interest. In the  
35  
36 following sections a time window up to 80 ms was interrogated after the laser pulse. Mass  
37  
38 spectra, kinetic time traces, and photoionization spectra are corrected for pre-photolysis signals  
39  
40 by subtracting the average ion counts in a 20 ms time window before the laser pulse. Having  
41  
42 subtracted this time-independent signal, the data in the figures represents the change of signals  
43  
44 as a result of the reactive species created by the laser pulse. Positive signals represent species  
45  
46 created because of the laser pulse, whereas negative signals correspond to species that are  
47  
48 depleted following irradiation. Finally, all signals are normalized to variations in VUV photon  
49  
50 flux that is monitored using a calibrated photodiode.  
51  
52  
53  
54  
55  
56  
57  
58  
59  
60

### 3. COMPUTATIONAL METHODS

Electronic structure calculations of neutral species and their cations leading to their optimized geometries have been performed using the Gaussian09 package with the B3LYP/CBSB7 method. Details about the calculations have been discussed elsewhere.<sup>41,42,46,47</sup> Heats of reaction, and adiabatic and vertical ionization energies, are calculated using the CBS-QB3 composite method.<sup>48,49</sup> Simulated Franck–Condon factors of isomer species are calculated at room temperature with the G09 package within the Franck–Condon approximation.<sup>44,50</sup> Although the experiments are performed at 373 K, the higher temperature does not result in significantly different vibrational populations. The calculated Franck–Condon factors are convolved with a Gaussian response function (FWHM of 0.025 eV) and integrated in order to simulate the photoionization spectra of the species assuming that direct ionization dominates the ionization process.

Saddle points for H- and CH<sub>3</sub>-transfer on the CH + CH<sub>3</sub>NH<sub>2</sub> potential energy surface (PES) are calculated using the CBS-QB3 composite method.<sup>48,49</sup> The saddle points are verified with intrinsic reaction coordinate (IRC) calculations at the B3LYP/6-31G(d) level of theory.

### 4. RESULTS

Under the present experimental conditions (4 Torr, 373 K, high dilution with inert gases), collisional quenching with the He (90%) and N<sub>2</sub> (10%) buffer gases will rapidly thermalize all the photolysis and reaction products to the temperature of the flow. Stabilization will not compete with dissociation of the reaction intermediates as long as the unimolecular dissociation occurs with a rate higher than the collision rate ( $<20 \times 10^6 \text{ s}^{-1}$ ). All the initial reaction adducts formed by addition of the CH radicals with unsaturated hydrocarbons are expected to have lifetimes shorter or on the order of their rotational period.<sup>40</sup> Assuming equally fast adduct isomerization and dissociation for reactions with amines under the above experimental conditions, stabilization of these intermediates through collisional quenching is not expected

1  
2  
3 to be a significant process. For these reasons, performing the experiments under thermal  
4 conditions provides information about the unimolecular isomerization and dissociation scheme  
5  
6 of the reaction intermediates.  
7  
8  
9

10 The kinetic traces and photoionization spectra are recorded by irradiating a mixture of  
11  $\text{CHBr}_3$  and the chosen amine in a  $\text{He}/\text{N}_2$  mixture at 248 nm. Along with  $\text{CH}(X^2\Pi, \nu=0)$ ,  
12 bromoform photodissociation produces  $\text{CH}(A^2\Delta)$ ,  $\text{CH}(X^2\Pi, \nu=1)$ ,  $\text{Br}$ ,  $\text{HBr}$ ,  $\text{CBr}$ ,  $\text{CHBr}$ ,  $\text{Br}_2$   
13 and  $\text{CHBr}_2$ . The  $\text{CH}(A^2\Delta)$  population decays radiatively within few microseconds after the  
14 laser pulse.<sup>51</sup> The vibrationally excited  $\text{CH}(X^2\Pi, \nu=1)$  radicals are efficiently quenched by  
15 adding nitrogen to the main flow.<sup>28,52</sup> The three body reaction of the  $\text{CH}(X^2\Pi, \nu=0)$  radical  
16 with molecular nitrogen is slow<sup>53</sup> at the pressure of the flow and is unlikely to affect the  
17 observed product distributions. Reactions of  $\text{CBr}$  with small unsaturated hydrocarbons are  
18 several orders of magnitude slower at the present temperature<sup>46,47,50,54-56</sup> than those for reactions  
19 of the  $\text{CH}$  radical.<sup>54,55,57,58</sup> Similarly slow kinetics between  $\text{CBr}$  and amines would allow  
20 discriminating between  $\text{CBr}$  and  $\text{CH}$  reaction products. At 248 nm the singlet  $\text{CHBr}$  carbene is  
21 expected to be formed in very low concentrations compared to the  $\text{CH}$  radical.<sup>59</sup> Its reaction  
22 with ammonia or the methyl-substituted amine reactants may form products through  $\text{HBr}$ -loss  
23 at the same  $m/z$  as the  $\text{CH}$  reaction products. There are no kinetic data available for the  
24 reactions of halocarbenes with amines. In the case of reactions with DMA and TMA, signals  
25 are observed at  $m/z$  values corresponding to dimethyl and trimethyl substituted amines plus  
26  $\text{C}^{79}\text{Br}/\text{C}^{81}\text{Br}$  isotopes. This indicates that the methyl substituted amines reacts with  $\text{CBr}$  to give  
27 the stabilized adduct, or with  $\text{CHBr}$  followed by a H-loss. The detection of brominated products  
28 suggests that the branching ratio for  $\text{Br}$  and/or  $\text{HBr}$  elimination is less than unity. Combined  
29 with the non-detection of signal at the  $m/z$  values of the brominated radicals, this suggests that  
30 the direct contribution of the  $\text{CBr}$  and  $\text{CHBr}$  reactions to signals at  $m/z$  corresponding  $\text{CH}$   
31 reaction products is therefore expected to be small.  
32  
33  
34  
35  
36  
37  
38  
39  
40  
41  
42  
43  
44  
45  
46  
47  
48  
49  
50  
51  
52  
53  
54  
55  
56  
57  
58  
59  
60

1  
2  
3 Successive reactions of the primary products with remaining radicals in the flow may  
4 lead to the formation of secondary products over the experimental reaction time. Because the  
5 reactions of CH with ammonia and amines are very fast,<sup>14</sup> it is possible to discriminate between  
6 primary and secondary reactions by inspecting the product temporal profiles. Figure S1  
7 displays typical kinetic traces obtained when irradiating a mixture of bromoform and MA in  
8 helium and nitrogen. The fast rise of the signals at  $m/z$  42, 43, and 57 indicates that these  
9 products are likely to be formed by a fast reaction while the slower rise observed at  $m/z$  58  
10 suggests that the corresponding product is from a slower or secondary reaction. In this section  
11 photoionization spectra are integrated over the 0–40 ms time range, whereas mass spectra  
12 integrations are restricted to 0–5 ms in order to minimize contribution from secondary or  
13 slower reactions. Products showing initial formation rates of less than  $500 \text{ s}^{-1}$  are assigned to  
14 secondary reactions and are not discussed further.

15  
16  
17  
18  
19  
20  
21  
22  
23  
24  
25  
26  
27  
28  
29  
30  
31 Time- and energy-resolved mass spectra are recorded by averaging at least 500 laser shots  
32 at each VUV photon energy, scanned over at least 1.5 eV with an energy step of 25 meV. Ar  
33 is used in a gas filter in order to absorb harmonics of the undulator radiation. All the amines  
34 used in this work have low absorption cross-sections at 248 nm ( $<1 \times 10^{-19} \text{ cm}^2$  for MA and  
35 DMA,  $\sim 1 \times 10^{-18} \text{ cm}^2$  for TMA)<sup>60-62</sup> leading to negligible dissociation of MA and DMA and less  
36 6% dissociation for TMA. Nonetheless, mass spectra of the  $\text{NH}_3$ , MA, DMA were  
37 systematically recorded with and without bromoform in order to confirm that no time-  
38 dependent signal was observed at the masses of the expected CH + amine reaction products.  
39 Although no background was recorded in the case of TMA, time resolved signal observed at  
40  $m/z$  58 is attributed to TMA photodissociation.

41  
42  
43  
44  
45  
46  
47  
48  
49  
50  
51  
52  
53  
54  
55  
56  
57  
58  
59  
60  
60 In the following sections, isomer products are identified based on their ionization  
energy and photoionization spectra. When experimental values are not available, the isomers  
are identified using the CBS–QB3 calculated ionization energies displayed in Table 1. The

1  
2  
3 difference of ionization energies between the C<sub>2</sub>H<sub>5</sub>N cis and trans stereoisomers is found to be  
4 less than 0.02 eV and the isomer identification is performed using the trans isomer. The  
5 photoion spectra are also fit with integrated experimental or integrated calculated (Franck–  
6 Condon factors) photoelectron spectra. The predicted spectra for individual isomers are  
7 displayed in Figure S1 (supplementary information). The integrated photoelectron spectra<sup>63</sup> do  
8 not distinguish between the cis and trans stereoisomers. The photoelectron spectra for the  
9 methyl substituted imines are integrated over the first two vibronic bands of the cation<sup>63</sup> and  
10 normalized to their maximum. Because of the large uncertainties in absolute photoionization  
11 cross sections between the different mass channel products, the data are not used to provide  
12 reaction product branching fractions. Nonetheless, isomeric branching ratios for a given mass  
13 channel are estimated on the assumption that isomers have equal ionization cross sections.<sup>64</sup> In  
14 the following paragraphs the displayed photoionization spectra for the individual isomers are  
15 weighted by their branching ratios.

34 Table 1. Ionization energies of imines and amino carbene isomers calculated using the CBS–  
35 QB3 method

		Imines RN=CR'R''				Amino carbene RR'N-CR''			
Formula	m/z	Isomer	IE (eV)	Isomer	IE (eV)	Isomer	IE (eV)	Isomer	IE (eV)
CH <sub>3</sub> N	29		9.94				8.39		
C <sub>2</sub> H <sub>5</sub> N	43		9.54 <sup>(1)</sup>		9.13		7.65		7.88 7.84
			8.83		9.19		7.38		7.53
C <sub>3</sub> H <sub>7</sub> N	57		8.83		9.19		7.38		7.53
C <sub>4</sub> H <sub>9</sub> N	71		8.42				6.91		

56 <sup>(1)</sup>Cis and trans isomers

#### 4.1 CH + NH<sub>3</sub>

Two H-loss exit channels of the CH + NH<sub>3</sub> reaction (R1) are possible, producing the imine HN=CH<sub>2</sub> and the amino carbene H<sub>2</sub>N–CH through channels R1a and R1b, respectively. The only other exothermic reaction exit channel predicted by Blitz *et al.*<sup>15</sup> is the formation of CH<sub>3</sub> + NH.

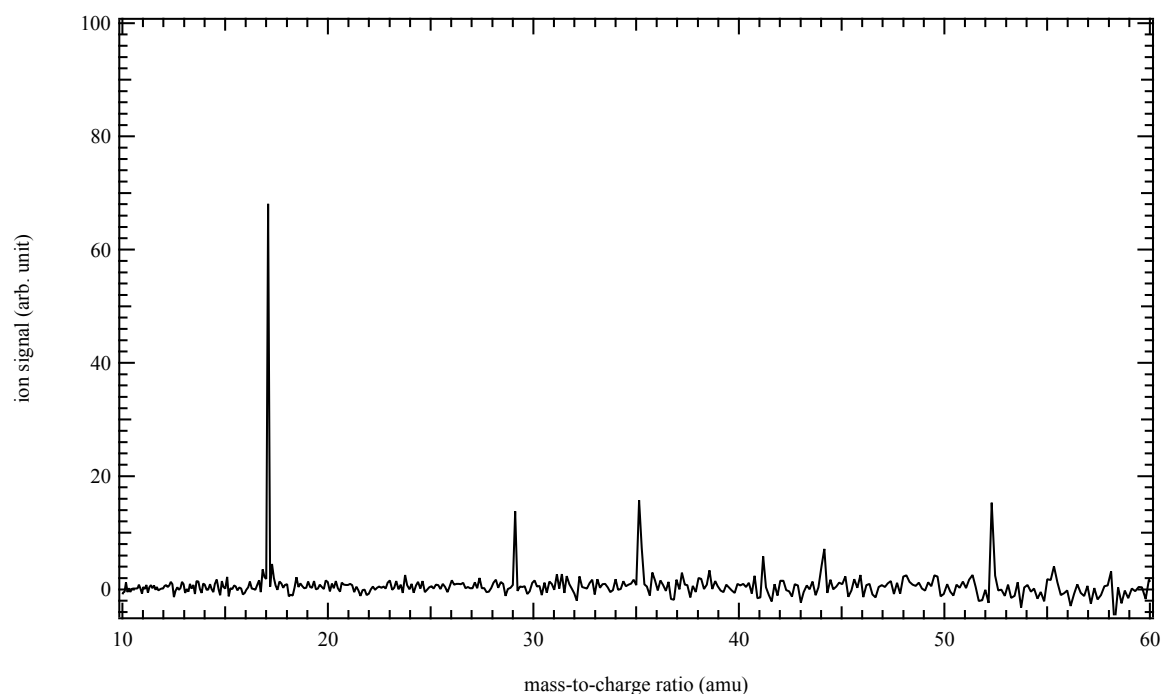


Figure 1. Mass spectrum obtained by photolysis of a CHBr<sub>3</sub> and NH<sub>3</sub> mixture in helium and nitrogen integrated over the 9.8-10.6 eV photon energy and the 0–5 ms time range.

Figure 1 displays the mass spectrum obtained by photolysis of a CHBr<sub>3</sub> and NH<sub>3</sub> mixture in helium integrated over the 9.8-10.6 eV photon energy and the 0–5 ms time range. The large signal at m/z 17 is likely due to fluctuations in the ammonia signal leading to a remaining positive signal after background subtraction. The main signals are observed at m/z 29, 35, and 52. The signal at m/z 29 displays a fast rise immediately after the laser pulse, as expected for a

CH + NH<sub>3</sub> reaction product. The temporal profiles of m/z 35 and 52 show a sharp signal rise starting about 4 ms after the laser pulse and displaying a rapid decay over the following 5 ms. Although the origin of these two signals is undetermined, NH<sub>3</sub>•H<sub>2</sub>O and 2NH<sub>3</sub>•H<sub>2</sub>O are the only species that match the observed m/z values. The formation of these clusters at 373 K is not favorable and the observed ions are more likely to come from dissociative ionization of higher mass neutral species. Additional signals (not shown here) are observed at m/z 79, 81, 104, and 106 corresponding to Br atoms and brominated compounds. The photoion signal at m/z 104 and 106 has a fast kinetic rise and shows an ion onset at about 10.3 eV corresponding to the photoionization energy of bromoacetylene.<sup>65</sup> Although there is no clear pathway leading to BrCCH formation in the reaction flow, its formation does not interfere with the detection of CH + NH<sub>3</sub> products. From this analysis, it is concluded that only the signal at m/z 29 originates from the CH + NH<sub>3</sub> reaction.

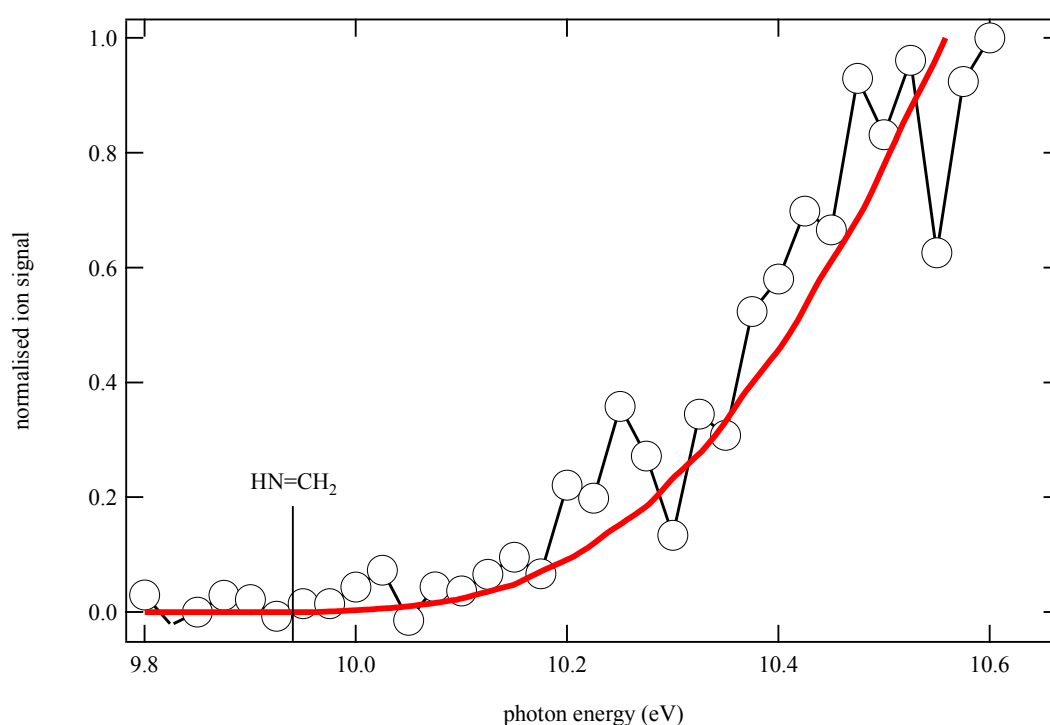


Figure 2. Photoionization spectrum of m/z 29 (open circles) obtained by photolysis of a CHBr<sub>3</sub> and NH<sub>3</sub> mixture in helium and nitrogen integrated over the 0–40 ms time range and displayed from 9.8 to 10.6 eV photon energy. The vertical line denotes the experimental ionization energy

of  $\text{HN}=\text{CH}_2$ .<sup>63</sup> The thick red line is the integrated experimental photoelectron spectrum of  $\text{HN}=\text{CH}_2$  from Bock *et al.*<sup>63</sup>

Figure 2 displays the photoionization spectrum of  $m/z$  29 integrated over the 0–40 ms time range. The good match between the experimental data (open circles) and the integrated experimental photoelectron spectrum of  $\text{HN}=\text{CH}_2$  (red thick line) from Bock *et al.*<sup>63</sup> confirms the formation of  $\text{HN}=\text{CH}_2$  in the reaction flow. As displayed in Table 1 the calculated  $\text{H}_2\text{N}-\text{CH}$  amino carbene ionization energy is 8.39 eV, well below that of the  $\text{HN}=\text{CH}_2$  isomer. The absence of signal below 9.9 eV confirms that the amino carbene isomer  $\text{H}_2\text{N}-\text{CH}$  is not formed in the reaction flow and that only R1a contributes to the reaction mechanism. Additional experiments were performed with deuterated bromoform as the radical precursor in order to provide information on isomerization pathways. The main  $\text{CD} + \text{NH}_3$  product signal is observed at  $m/z$  30 with no significant signal at  $m/z$  29, indicating an absence of D loss from the initial adduct. The photoionization spectrum of  $m/z$  30 is identical to that of  $m/z$  29 from the  $\text{CH} + \text{NH}_3$  reaction.

#### 4.2 CH + $\text{CH}_3\text{NH}_2$

The reaction of the CH radical with MA (R2) may proceed both by H- (R2a, b, c, and d) or  $\text{CH}_3$ -loss (R2e and f) to form imines (R2a, b, and e) or amino carbenes (R2c, d, and f) at  $m/z$  43 and 29. The enthalpy of reaction for producing trans- vs. cis- $\text{HN}=\text{CHCH}_3$  or trans- vs. cis- $\text{CH}_3\text{HN}-\text{CH}$  stereoisomers differs by less than 3  $\text{kJ mol}^{-1}$ ; the enthalpies of reaction given in R2a and R2c are for the trans isomers. All the exit pathways are exothermic with formation of the imines being at least 100  $\text{kJ mol}^{-1}$  more exothermic than the amino carbenes.

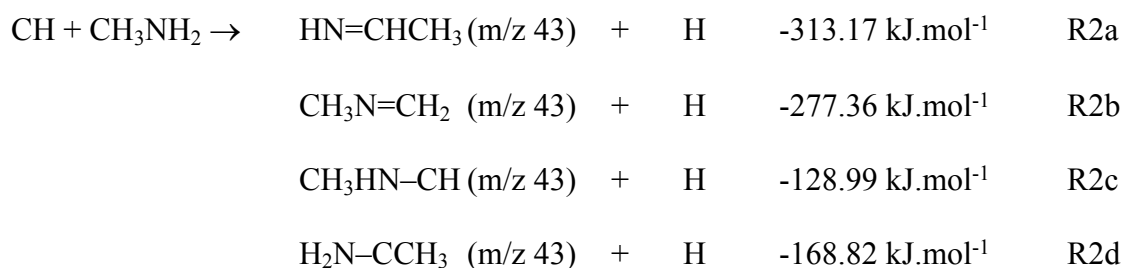




Figure 3 displays the photoionization spectrum of  $m/z$  29 (open circles) obtained by photolysis of a  $\text{CHBr}_3$  and  $\text{CH}_3\text{NH}_2$  mixture in helium and nitrogen integrated over the 0–40 ms time range. The thick red line is the integrated photoelectron spectrum of  $\text{HN}=\text{CH}_2$  from Bock *et al.*<sup>63</sup> The good match between the experimental data and the integrated photoelectron spectrum as well as the absence of signal below 9.9 eV suggest that only the imine isomer is formed in the reaction flow.

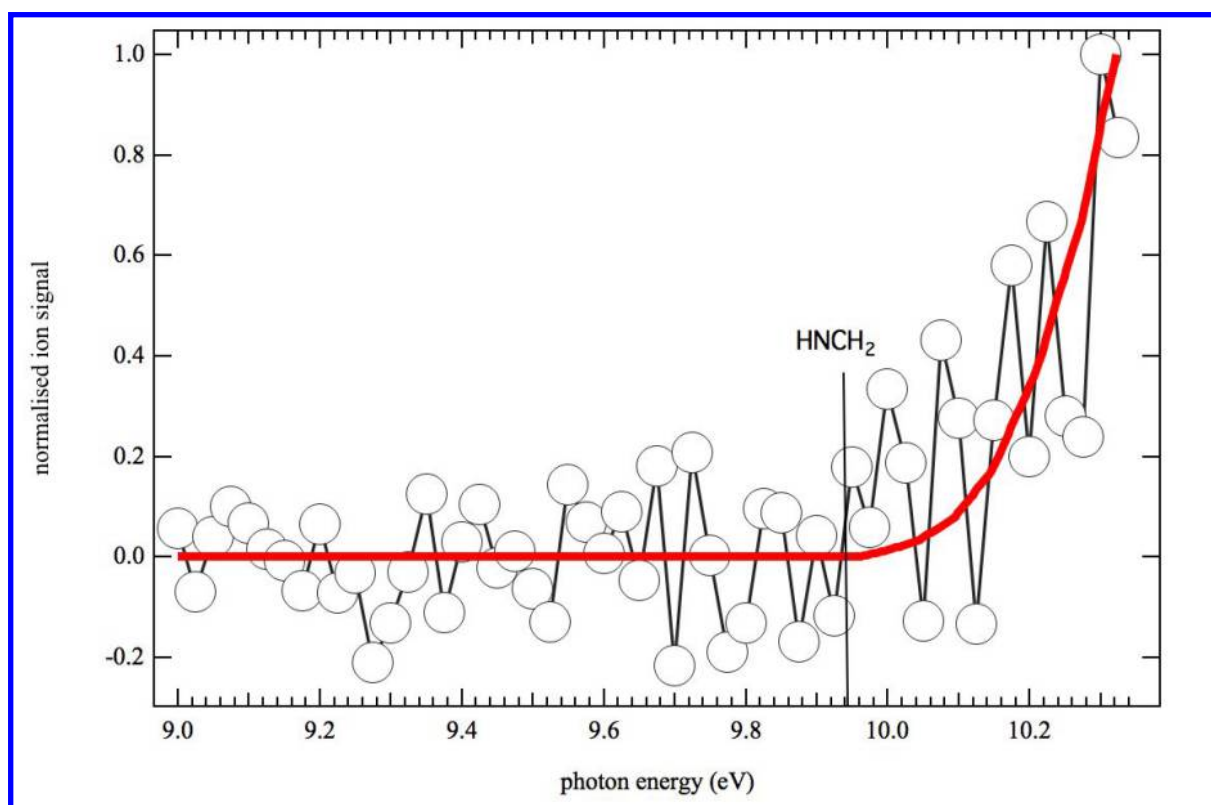
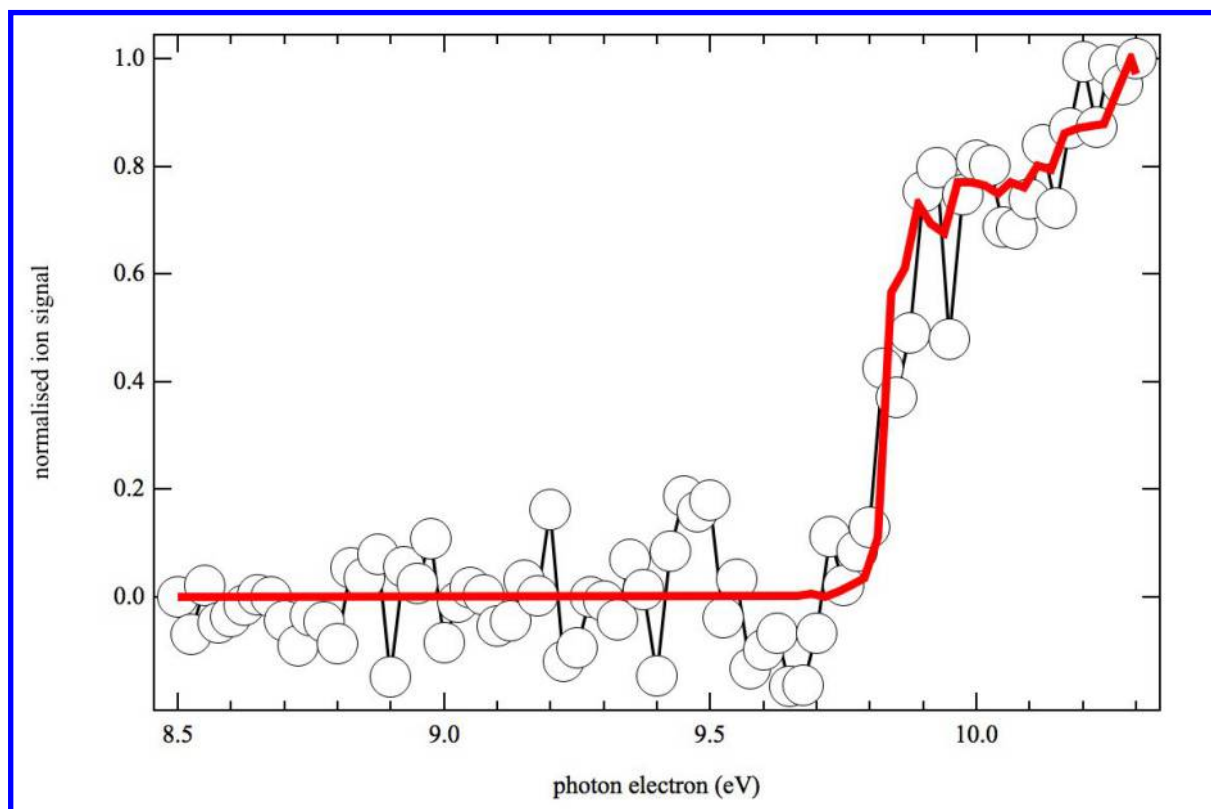


Figure 3. Photoionization spectrum of  $m/z$  29 (open circles) obtained by photolysis of a  $\text{CHBr}_3$  and  $\text{CH}_3\text{NH}_2$  mixture in helium and nitrogen integrated over the 0–40 ms time range and displayed from 9.0 to 10.3 eV photon energy. The thick red line is the integrated photoelectron spectrum of  $\text{HN}=\text{CH}_2$  from Bock *et al.*<sup>63</sup>

Figure 4 displays the photoion signal at  $m/z$  15 (open circles) integrated over the 0–40 ms time range obtained by photolysis of a  $\text{CHBr}_3$  and  $\text{CH}_3\text{NH}_2$  mixture. The data is superposed to the

1  
2  
3 experimental spectrum of the methyl radical (red line).<sup>66</sup> The good match confirms the  
4  
5 formation of CH<sub>3</sub> radical in the reaction flow.  
6  
7  
8  
9



35 Figure 4. Photoion signal at  $m/z$  15 (open circles) integrated over the 0–40 ms time range  
36 obtained by photolysis of a CHBr<sub>3</sub> and CH<sub>3</sub>NH<sub>2</sub> mixture in helium and nitrogen displayed from  
37 8.5 to 10.3 eV photon energy. The thick red line is the absolute spectrum (solid red line) of the  
38 methyl radical (CH<sub>3</sub>) obtained by Savee *et al.*<sup>66</sup>  
39  
40  
41  
42  
43

44 Figure 5 displays the photoionization spectra obtained at  $m/z$  43 recorded under the  
45 same experimental conditions as those of Figures 3 and 4. The purple solid line is a fit to the  
46 data using normalized integrated photoelectron spectra of two methylimine isomers:  
47 CH<sub>3</sub>N=CH<sub>2</sub> (blue dashed line) and HN=CHCH<sub>3</sub> (red dotted line),<sup>63</sup> assuming equal  
48 photoionization cross sections after the first two vibronic bands. The fit to the data returns a  
49 CH<sub>3</sub>N=CH<sub>2</sub>:HN=CHCH<sub>3</sub> branching ratio of 0.9:1. The absence of onset at the ionization  
50 energy of the CH<sub>3</sub>N=CH<sub>2</sub> is likely due to the poor Franck–Condon overlap between the neutral  
51 and cation vibronic ground states.  
52  
53  
54  
55  
56  
57  
58  
59  
60

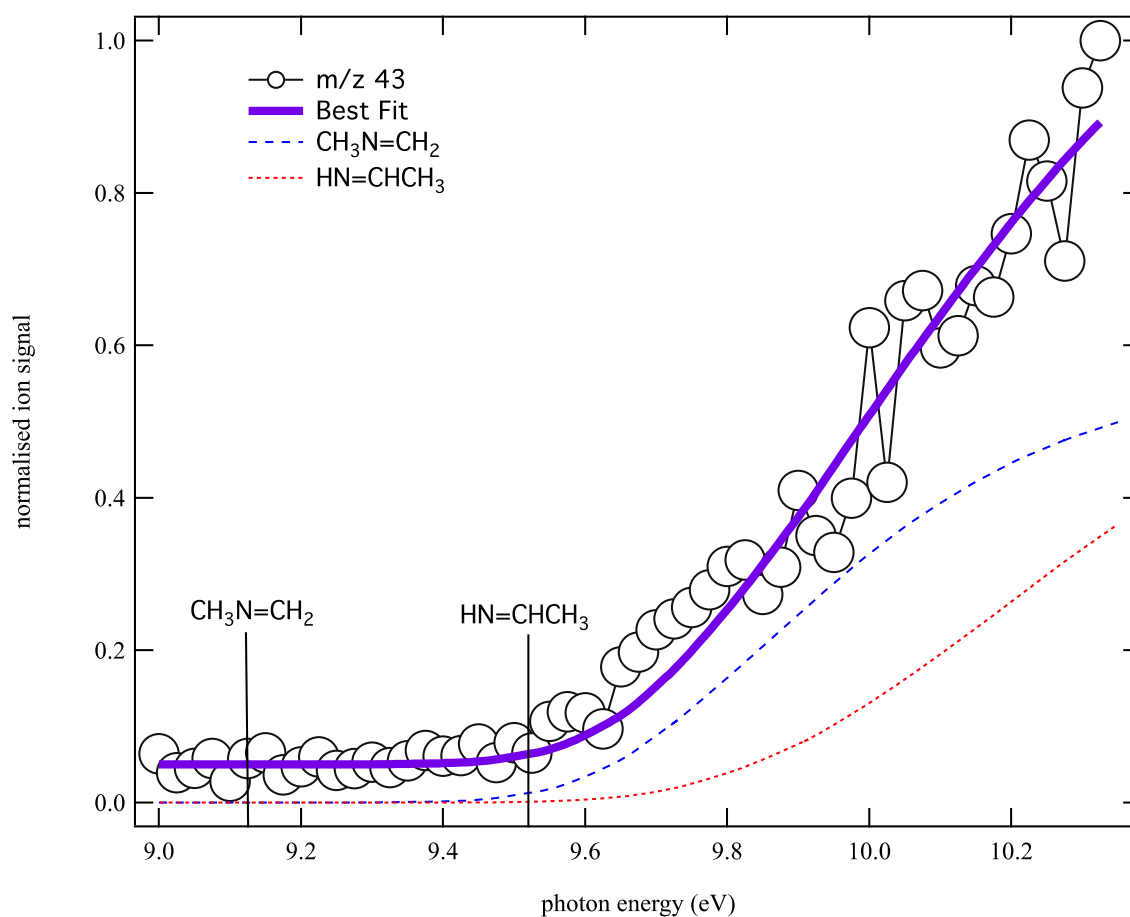


Figure 5. Photoionization spectrum at  $m/z$  43 (open circles) obtained by photolysis of a  $\text{CHBr}_3$  and  $\text{CH}_3\text{NH}_2$  mixture in helium and nitrogen integrated over the 0–40 ms time range. The purple solid line is a fit to the data using the integrated photoelectron spectra of  $\text{CH}_3\text{N}=\text{CH}_2$  (blue dashed line),  $\text{HN}=\text{CHCH}_3$  (red dotted line) from Bock *et al.*<sup>63</sup> The best fit to the data is obtained for a  $\text{CH}_3\text{N}=\text{CH}_2$ : $\text{HN}=\text{CHCH}_3$  branching ratio of 0.9:1.

In Figure 5, a small ion signal is observed from 9.0 – 9.1 eV, below the energy of both imine isomers. Inspection of the kinetic traces reveals that the corresponding ions are detected only after irradiation of the flow by the laser pulse. This signal below 9.1 eV remains constant after the laser pulse, which is uncharacteristic of reactive carbene molecules. No signals are detected at the  $m/z$  corresponding to the brominated adducts, and the offset is therefore unlikely to be due to dissociative ionization of higher mass products. The constant signal offset below the energy of the methylimine isomers does not enable us to unequivocally rule out the

formation of the amino carbene isomers, but should not affect the methylimine branching ratios.

### 4.3 CH + (CH<sub>3</sub>)<sub>2</sub>NH

The reaction of the CH radical with dimethyl amine may lead to a total of 8 exothermic exit channels, through H-loss (R3a, a' b, c, and d) and CH<sub>3</sub>-loss (R3e, f, g, and h). The enthalpy in R3e is for the trans isomer. As for the reaction with MA, formation of the methyl amino carbenes (R3c, d, g, and h) is found to be less thermodynamically favorable by at least 100 kJ.mol<sup>-1</sup>.

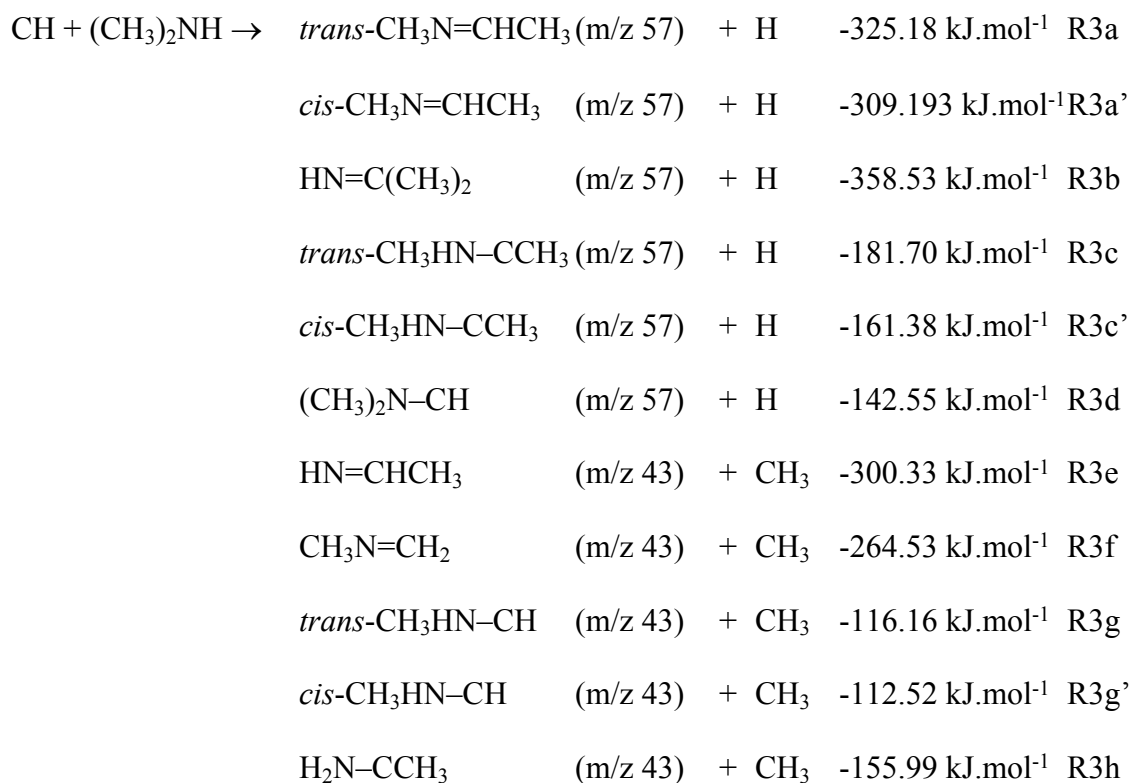


Figure 6 displays the mass spectrum obtained by photolysis of a CHBr<sub>3</sub> and (CH<sub>3</sub>)<sub>2</sub>NH mixture in helium and nitrogen integrated over the 8.5-10.6 eV photon energy and the 0–5 ms time range. The main signals are detected at m/z 15, 42, 43, 57 and 58. The signal at m/z 58 increases more slowly (400 s<sup>-1</sup>) than the other signals and is likely not a direct product of the CH + DMA reaction. The photoion spectrum of m/z 42 shows an ionization onset at ~9.7 eV with a photoionization spectrum characteristic of propene (C<sub>3</sub>H<sub>6</sub>).

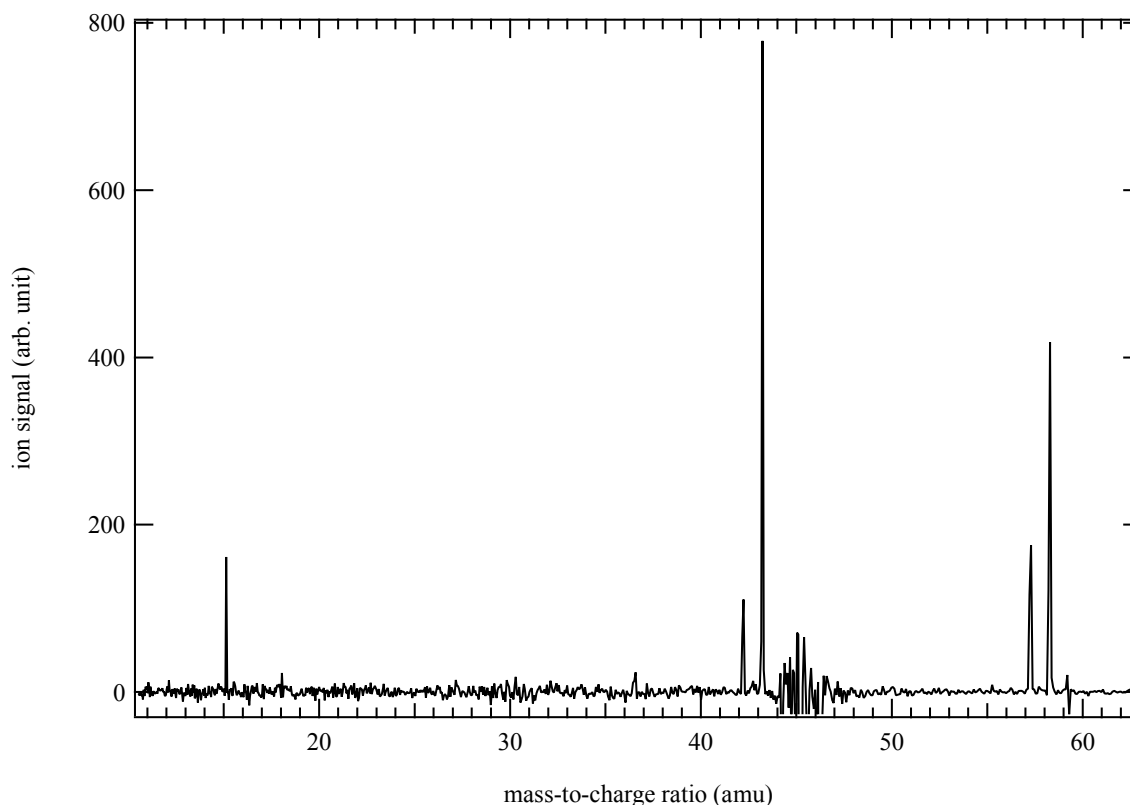


Figure 6. Mass spectrum obtained by photolysis of a  $\text{CHBr}_3$  and  $(\text{CH}_3)_2\text{NH}$  mixture in helium and nitrogen integrated over the 8.5-10.6 eV photon energy and the 0–5 ms time range.

Figure 7 displays the photoion signal at  $m/z$  43 (open circles) integrated over the 0–40 ms time range from the same experiment. The purple solid line is a fit to the data using the integrated photoelectron spectra of  $\text{CH}_3\text{N}=\text{CH}_2$  (blue dashed line) and  $\text{HN}=\text{CHCH}_3$  (red dotted line) from Bock *et al.*<sup>63</sup> The best fit to the data is obtained for a  $\text{CH}_3\text{N}=\text{CH}_2:\text{HN}=\text{CHCH}_3$  ratio of 0.7:1. No ion signal is detected at low energy, suggesting that no methyl amino carbene isomers are formed. The expected mass 43 co-product, the methyl radical, is detected at  $m/z$  15 with a photoionization spectrum identical to that displayed in Figure 4.

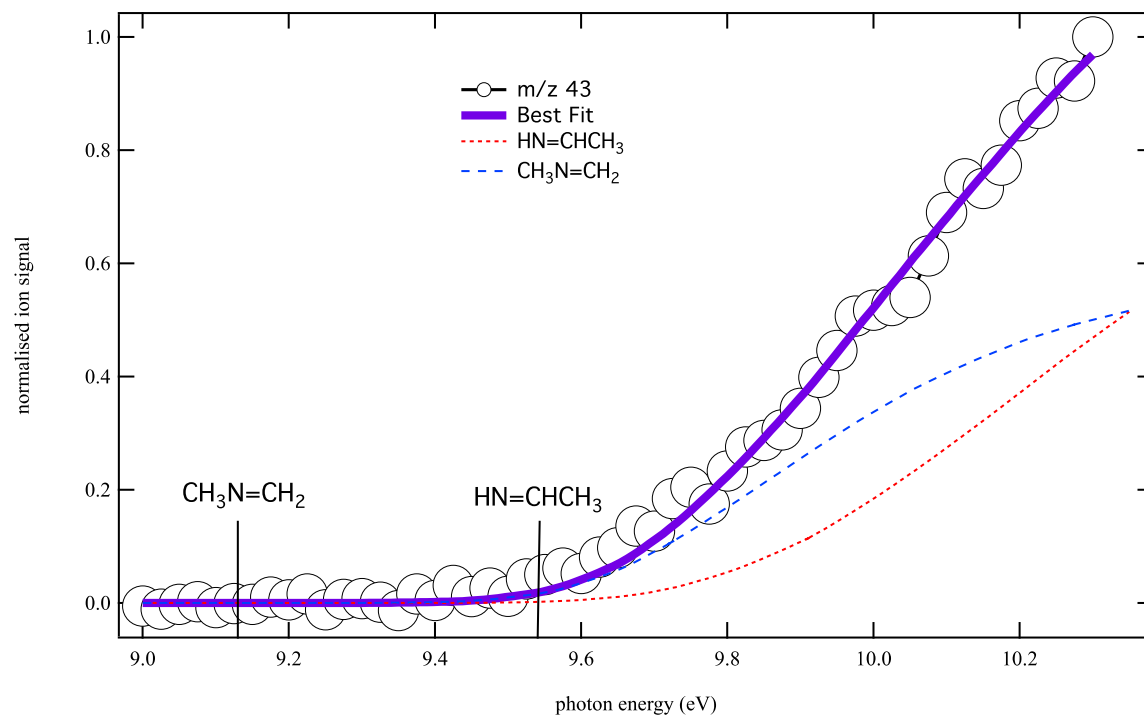


Figure 7. Photoionization spectrum at  $m/z$  43 (open circles) obtained by photolysis of a  $\text{CHBr}_3$  and  $(\text{CH}_3)_2\text{NH}$  mixture in helium and nitrogen integrated over the 0–40 ms time. The purple solid line is a fit to the data using the integrated photoelectron spectra of  $\text{CH}_3\text{N}=\text{CH}_2$  (blue dashed line) and  $\text{HN}=\text{CHCH}_3$  (red dotted line) from Bock *et al.*<sup>63</sup> The best fit to the data is obtained for a  $\text{CH}_3\text{N}=\text{CH}_2:\text{HN}=\text{CHCH}_3$  branching ratio of 0.7:1.

Figure 8 displays the photoionization spectrum at  $m/z$  57 (open circles) recorded under the same experimental conditions as those of Figure 6 and 7. The purple solid line is a fit to the data using the integrated photoelectron spectra of  $\text{HN}=\text{C}(\text{CH}_3)_2$  (red dashed line) from Bock *et al.*<sup>63</sup> as well as integrated Franck-Condon factors for the *trans*- (blue dotted line) and *cis*- (blue dotted and dashed line)  $\text{CH}_3\text{N}=\text{CHCH}_3$  isomers. There is a constant signal offset below the ionization energies of the *cis* and *trans* dimethylimine stereoisomers. Although the observed signal could be attributed to the dimethyl amino-carbenes  $\text{CH}_3\text{HN}-\text{CCH}_3$  and  $(\text{CH}_3)_2\text{N}-\text{CH}$ , the  $m/z$  57 temporal profile below the energy of the  $\text{CH}_3\text{N}=\text{CHCH}_3$  dimethylimine isomers displays a constant signal after its formation by the laser pulse. Such time-trace is unlikely for reactive carbene compounds. Signals are also detected at  $m/z$  121/123, 122/124 and 135/137,

likely corresponding to brominated compounds. No signals are observed at  $m/z$  136/138 or 137/139 values corresponding to the  $\text{CHBr/CBr} + \text{DMA}$  reaction adducts. Dissociative ionization of singly brominated products through  $\text{HBr}$  or  $\text{H}$  loss is therefore not likely to explain the observed signal offset. Alternatively, the offset could be due to dissociative ionization of  $\text{CBr}_2$  reaction adducts through  $\text{Br}_2$  loss. The best fit to the data using a constant offset before the ionization energy of the  $\text{CH}_3\text{N}=\text{CHCH}_3$  dimethylimine isomers returns a  $\text{trans-CH}_3\text{N}=\text{CHCH}_3$ : $\text{cis-CH}_3\text{N}=\text{CHCH}_3$ : $\text{HN}=\text{C}(\text{CH}_3)_2$  of 1:0.2:0.8.

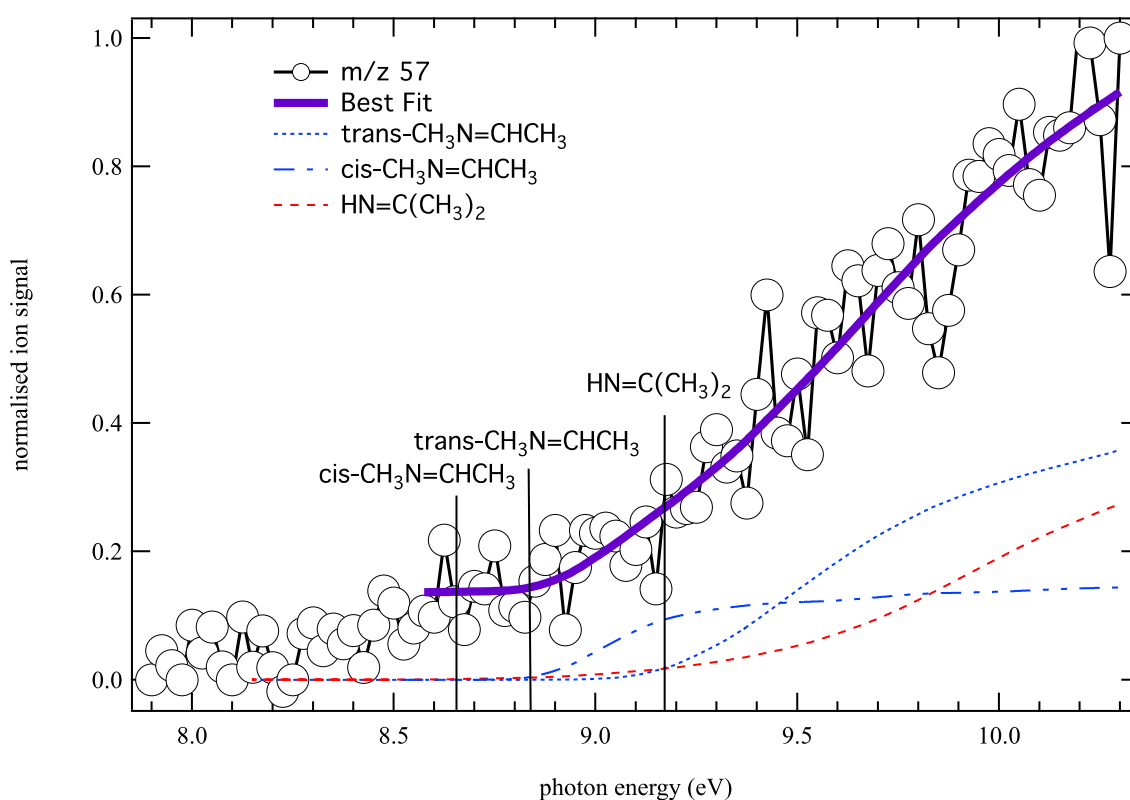
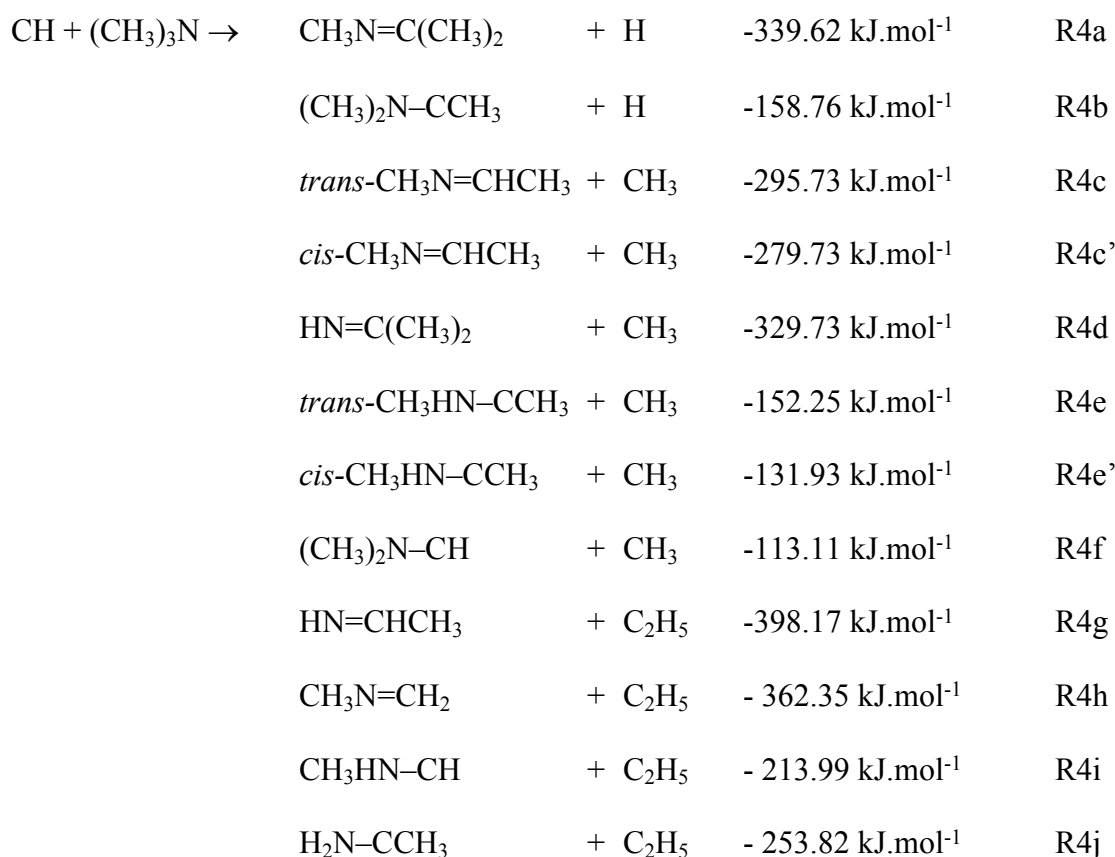


Figure 8. Photoion signal at  $m/z$  57 (open circles) obtained by photolysis of a  $\text{CHBr}_3$  and  $(\text{CH}_3)_2\text{NH}$  mixture in helium and nitrogen integrated over the 0–40 ms time range and displayed from 7.8 to 10.2 eV photon energy. The purple solid line is a fit to the data using the integrated photoelectron spectra of  $\text{HN}=\text{C}(\text{CH}_3)_2$  (red dashed line) as well as the  $\text{trans-}$  (blue dotted line) and  $\text{cis-}$  (blue dotted and dashed line)  $\text{CH}_3\text{N}=\text{CHCH}_3$ . The best fit to the data is obtained for a branching ratio  $\text{trans-CH}_3\text{N}=\text{CHCH}_3$ : $\text{cis-CH}_3\text{N}=\text{CHCH}_3$ : $\text{HN}=\text{C}(\text{CH}_3)_2$  of 1:0.2:0.8.

#### 4.4 CH + (CH<sub>3</sub>)<sub>3</sub>N

The 6 most likely exit channels for the CH reaction with TMA are formation of the fully methyl substituted imine and amino carbene, detected at m/z 71 (R4a, and b), as well as the dimethylimines (R4c, c' and d) and dimethyl amino carbenes (R4e and f) at m/z 57. The enthalpies in R4g and R4i are for the trans isomers. Formation of the methyl substituted imines or amino carbene, detected at m/z 43, by loss of a C<sub>2</sub>H<sub>5</sub> radical are also exothermic.



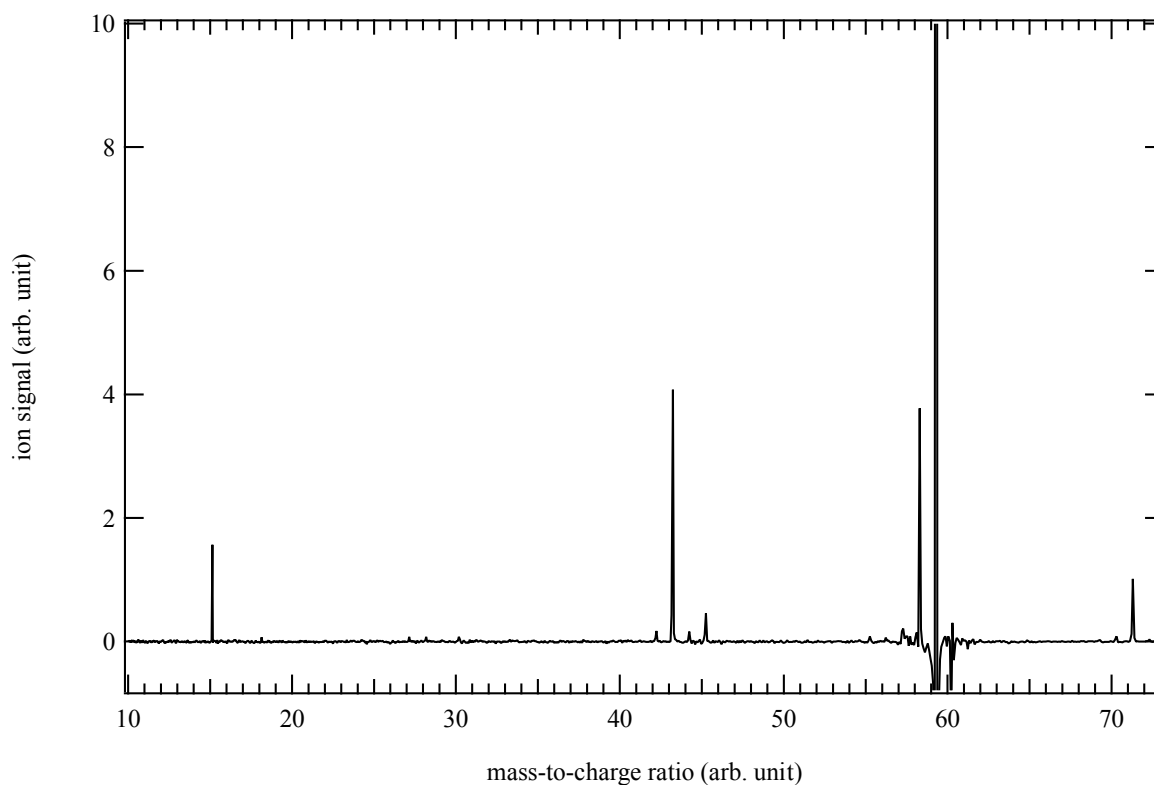


Figure 9. Mass spectrum obtained by photolysis of a  $\text{CHBr}_3$  and  $(\text{CH}_3)_3\text{NH}$  mixture in helium and nitrogen integrated over the 8.2–10.3 eV photon energy and the 0–5 ms time range.

Figure 9 displays the mass spectrum obtained by photolysis of a  $\text{CHBr}_3$  and  $(\text{CH}_3)_3\text{N}$  mixture integrated over the 8.2–10.3 eV photon energy and the 0–5 ms time range. The main signals are detected at  $m/z$  15, 43, 58, 59, and 71. Signal at  $m/z$  59 is likely to come from the incomplete baseline subtraction of the large TMA signal. As for the reaction with DMA, signal at  $m/z$  15 is identified as coming from ionization of the methyl radical formed in the reaction flow. Although not as prominent as for reaction R3, signal at  $m/z$  42 is identified as propene ( $\sim 9.7$  eV). Signal at  $m/z$  58 displays a fast kinetics and a photoionization spectrum with a lower ionization energy onset ( $\sim 8.9$  eV) than that discussed in Section 4.3 for the bromofrom/DMA mixture at the same  $m/z$  value. After a fast rise, the signal is found to decay rapidly, within 4 ms after the laser pulse, which is not consistent with the formation of a closed shell molecule

1  
2  
3 from the CH + TMA reaction. In this case the signal observed at  $m/z$  58 could come from the  
4  
5 dissociative ionization of a higher-mass radical species or direct photodissociation of TMA.  
6  
7

8 The photoionization spectrum recorded at  $m/z$  43 for TMA and bromoform is similar to  
9  
10 those recorded at the same  $m/z$  for DMA and bromoform and suggests the formation of  
11  
12  $\text{CH}_3\text{N}=\text{CH}_2$ . No signal is detected at  $m/z$  29 for the expected  $\text{C}_2\text{H}_5$  coproduct. In the case of  
13  
14 the bromoform/TMA mixture, there is a very small signal at  $m/z$  57 (Figure 9), representing  
15  
16 less than 10% of the sum of all the signals at  $m/z$  43, 57 and 71. Its photoionization spectrum  
17  
18 is similar to that displayed in in Figure 8 (open circles). The good match between the two  
19  
20 experimental photoion spectra confirms formation of the dimethylimine isomers in the flow,  
21  
22 although with a much lower fraction than for the CH + DMA reaction.  
23  
24  
25

26 Figure 10 displays photoionization spectrum of  $m/z$  71 (open circles) recorded under  
27  
28 the same experimental conditions as Figures 9. A large signal offset is observed below 8.5 eV.  
29  
30 As for the reaction with MA and DMA, the temporal profile of the ions detected at low energy  
31  
32 is constant after their formation upon irradiation by the laser pulse. In the case of reaction with  
33  
34 TMA, signals are detected at  $m/z$  150/152 as well as 151/153 possibly corresponding to the  
35  
36  $\text{CHBr}/\text{CBr}$  reaction adducts or products. Dissociative ionization of these larger mass molecule  
37  
38 may contribute to the observed large signal. The lack of time dependence of the low energy  
39  
40  $m/z$  71 suggests that the reactive trimethyl amino carbene isomers are not contributing  
41  
42 significantly to the CH + TMA reaction products. Including a constant offset, the  
43  
44 photoionization spectrum in Figure 10 is consistent with the formation of the  $\text{CH}_3\text{N}=\text{C}(\text{CH}_3)_2$   
45  
46 isomer.  
47  
48  
49  
50  
51  
52  
53  
54  
55  
56  
57  
58  
59  
60

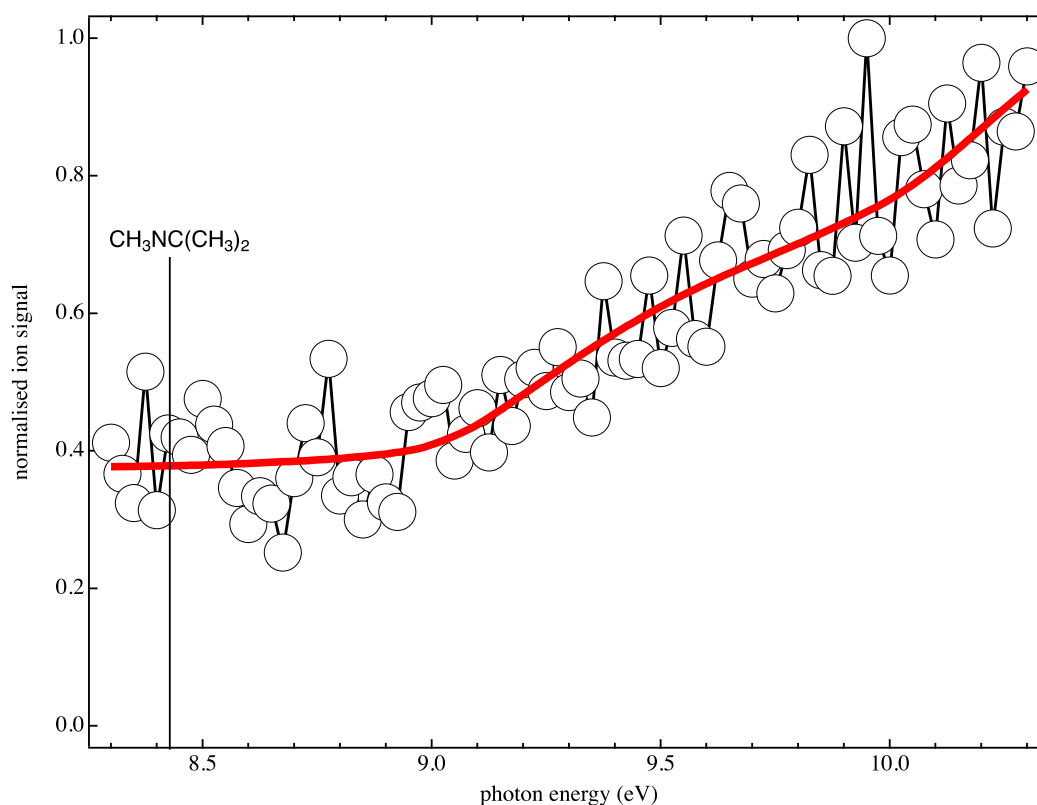


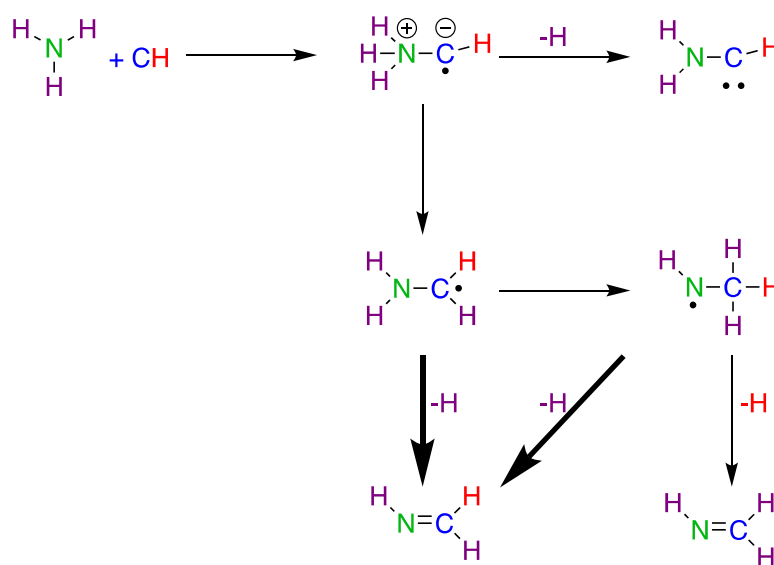
Figure 10. Photoionization spectrum of  $m/z$  71 (open circles) obtained by photolysis of a  $\text{CHBr}_3$  and  $(\text{CH}_3)_3\text{NH}$  mixture in helium and nitrogen integrated over the 0–40 ms time range. The red solid line is the integrated photoelectron spectra  $\text{CH}_3\text{N}=\text{C}(\text{CH}_3)_2$  (red dotted line) from Bock *et al.*<sup>63</sup>.

## 5. DISCUSSION

### 5.1 Reaction mechanisms

The reaction of the CH radical with  $\text{NH}_3$  has been studied both experimentally and theoretically.<sup>15</sup> The MCSCF/CASSCF PES reveals that the initial  $\text{H}_3\text{N}-\text{CH}$  complex is formed by a Lewis acid/base-type reaction for which the nitrogen donates electrons to the CH Lewis acid. This donor–acceptor interaction results in positive and negative charges on the nitrogen and carbon atoms, respectively. A similar mechanism has been proposed for reactions of singlet carbene compounds ( $\text{CH}_2$ ,  $\text{CHCl}$ ,  $\text{CHF}$ ) with amines.<sup>67</sup> According to the  $\text{CH} + \text{NH}_3$  PES,<sup>15</sup> the dative  $\text{H}_3\text{N}-\text{CH}$  complex is formed with no energy barrier leading to kinetics mainly controlled by long-range interactions. Scheme 1 displays the mechanism proposed by Blitz *et al.*<sup>15</sup> The

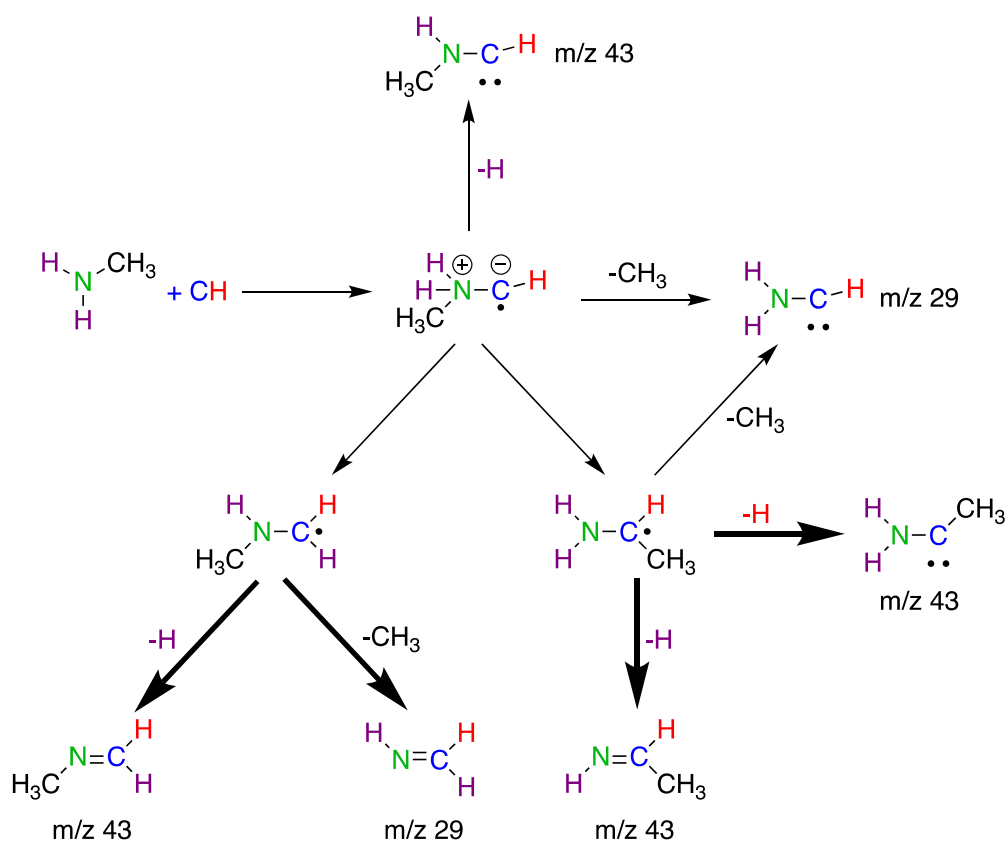
1  
2  
3 initial  $\text{H}_3\text{N}-\text{CH}$  adduct may directly dissociate to  $\text{H}_2\text{N}-\text{CH} + \text{H}$  or isomerize through H-atom  
4 transfer to form a more stable  $\text{H}_2\text{N}-\text{CH}_2$  reaction intermediate. The most likely fate of the  $\text{H}_2\text{N}-$   
5  $\text{CH}_2$  intermediate is dissociation to  $\text{HN}=\text{CH}_2 + \text{H}$ , either directly or through a second H-atom  
6 transfer followed by H-atom loss. The detection of only  $\text{HN}=\text{CH}_2$  isomer as a product of the  
7  $\text{CH} + \text{NH}_3$  reaction in the present study agrees with the RRKM-ME branching ratios calculated  
8 on the PES by Blitz et al.<sup>15</sup> in which the H-loss from the initial  $\text{H}_3\text{N}-\text{CH}$  complex is predicted  
9 not to be a competitive channel.  
10  
11  
12  
13  
14  
15  
16  
17  
18



Scheme 1

38  
39  
40  
41 The only channel leading to the imine  $\text{HN}=\text{CH}_2$  through elimination of the hydrogen  
42 atom initially on the carbon atom involves two successive H-transfers from the nitrogen atom  
43 to the carbon atom to form the  $\text{HN}-\text{CH}_3$  intermediate. In the case of the  $\text{CD} + \text{NH}_3$  reaction,  
44 assuming that the deuteration has no effect on the unimolecular dissociation rate, dissociation  
45 of the  $\text{HN}-\text{CH}_2\text{D}$  intermediate would lead to a 2:1 ratio for  $\text{HN}=\text{CHD}:\text{HN}=\text{CH}_2$ . The detection  
46 of mainly  $m/z$  30 from the  $\text{CD} + \text{NH}_3$  reaction suggests that the second H transfer does not  
47 compete with the direct dissociation of the  $\text{H}_2\text{N}-\text{CHD}$  intermediate. The good agreement  
48 between the present work and the RRKM-ME performed on the high-level PES supports the  
49 dative-bond mechanism proposed by Blitz et al. for the  $\text{CH} + \text{NH}_3$  reaction.  
50  
51  
52  
53  
54  
55  
56  
57  
58  
59  
60

Although there is no theoretical information about the  $\text{CH} + \text{NH}_2\text{CH}_3$  PES, Zabarnick *et al.*<sup>14</sup> suggest that the reaction proceeds through insertion of the CH radical into N–H or C–H bonds followed by a rapid decomposition of the reaction intermediates. Zabarnick *et al.* proposed these mechanisms based on the comparison of the measured reaction rate coefficients with those of the  $\text{CH} + \text{NH}_3$  and  $\text{CH} + \text{C}_2\text{H}_6$  reactions. In view of the PES calculated for the  $\text{CH} + \text{NH}_3$ ,<sup>15</sup> as well as the proposed mechanism for  $\text{CH}_2$ , CHF, and CHCl singlet carbene with MA,<sup>67</sup> it is likely that the reaction may also proceed through the formation of a dative intermediate. Direct insertion into a C–H bond of the methyl group is likely to be a minor entrance channel as observed for unsaturated hydrocarbons.<sup>40</sup>



Scheme 2

Scheme 2 displays a proposed mechanism for the  $\text{CH} + \text{CH}_3\text{NH}_2$  reaction starting from the formation of the dative  $\text{CH}_3\text{H}_2\text{N}-\text{CH}$  intermediate. Bold arrows correspond to observed channels. The detection of  $m/z$  15, 29, and 43 supports the fact that the reaction proceeds

1  
2  
3 through both H- and CH<sub>3</sub>-loss. We have no evidence to support direct dissociation of the  
4  
5 CH<sub>3</sub>NH<sub>2</sub>-CH dative adduct by H-loss to form the CH<sub>3</sub>HN-CH methyl amino carbene at m/z  
6  
7 43 or CH<sub>3</sub>-loss to form the H<sub>2</sub>N-CH isomer at m/z 29. The dative intermediate is therefore  
8  
9 more likely to isomerize through either H- or CH<sub>3</sub>-transfer to give CH<sub>3</sub>HN-CH<sub>2</sub> and/or H<sub>2</sub>N-  
10  
11 CHCH<sub>3</sub> intermediates. The so-formed CH<sub>3</sub>HN-CH<sub>2</sub> isomer can lose either a H atom or a CH<sub>3</sub>  
12  
13 group to give the detected CH<sub>3</sub>N=CH<sub>2</sub> and HN=CH<sub>2</sub> final imine products. The H<sub>2</sub>N-CHCH<sub>3</sub>  
14  
15 intermediate resulting from the CH<sub>3</sub> transfer can lose one of the two H-atoms on the nitrogen  
16  
17 to form the cis or trans HN=CHCH<sub>3</sub> imines or the H-atom initially on the carbon atom of the  
18  
19 CH radical to form the H<sub>2</sub>N-CCH<sub>3</sub> amino carbene. Loss of the methyl group on the carbon  
20  
21 CH radical to form the H<sub>2</sub>N-CH amino carbene. We have no evidence of the H<sub>2</sub>N-CH and H<sub>2</sub>N-  
22  
23 CHCH<sub>3</sub> amino carbene in the reaction flow.

24  
25  
26  
27  
28  
29 The 0.9:1 branching ratio for CH<sub>3</sub>N=CH<sub>2</sub>:HN=CHCH<sub>3</sub> at m/z 43 (Figure 5) suggests  
30  
31 that the CH<sub>3</sub>-transfer may compete with the H-transfer following the formation of the initial  
32  
33 dative adduct. In recent literature, methyl-group transfers have not been necessary to explain  
34  
35 the observed reaction products from a CH reaction with saturated or unsaturated  
36  
37 hydrocarbons.<sup>40</sup> In order to gain additional knowledge about the likelihood of the methyl-group  
38  
39 transfer, the saddle points for the H- and CH<sub>3</sub>-transfers from the CH<sub>3</sub>H<sub>2</sub>N-CH intermediate  
40  
41 have been calculated at the CBS-QB3 level of theory. Figure 11 displays the energetics for the  
42  
43 initial reaction adduct, the two isomers resulting from the H- and CH<sub>3</sub>-transfer, as well as the  
44  
45 corresponding saddle points. All the energies are calculated relatively to that of the reactants.  
46  
47 At this level of theory the saddle point for the H-transfer is found to be below that of the  
48  
49 reactants while that for the CH<sub>3</sub>-transfer is 17.1 kJ.mol<sup>-1</sup> above that of CH + CH<sub>3</sub>NH<sub>2</sub>.  
50  
51  
52  
53  
54  
55  
56  
57  
58  
59  
60

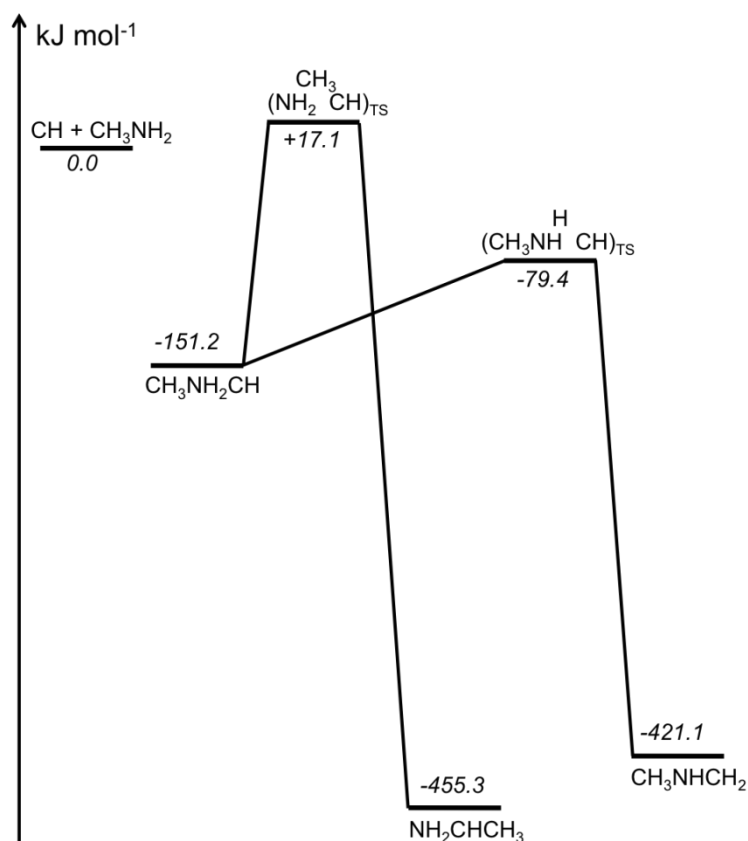
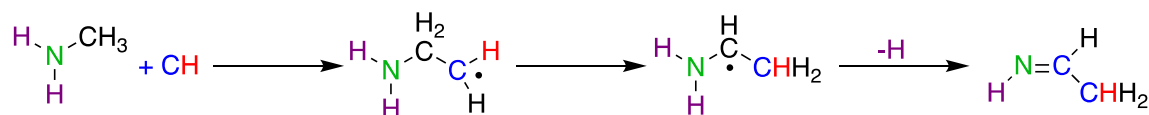


Figure 11. C<sub>2</sub>H<sub>6</sub>N stationary points calculated using the CBS–QB3 method.

Estimates for absolute uncertainty of the CBS–QB3 method<sup>68</sup> make it unlikely that the CBS–QB3 saddle point energy for methyl transfer lies below the reactant energy. Although the CBS–QB3 method has been shown not to be appropriate to calculate the energy of a dative interaction,<sup>68,69</sup> the relative energies of the two saddle points displayed in Figure 11 show that the CH<sub>3</sub> transfer is energetically less favorable than the H-transfer. As suggested for B–N dative bonds, the MP2 method and higher level methods may be more appropriate for such studies.<sup>69</sup> The detection of HN=CHCH<sub>3</sub> from the CH + CH<sub>3</sub>NH<sub>2</sub> reaction may be explained by a lowering of the CH<sub>3</sub>-transfer transition state below that of the reactants due to the dative interaction. Alternatively, direct insertion of the CH radical into the N–C or a methyl C–H bond could become a competitive entrance channel. Scheme 3 displays a possible mechanism for radical insertion into a C–H bond requiring only one H-atom transfer (and no CH<sub>3</sub> transfer) to form the H<sub>2</sub>N–CHCH<sub>3</sub> intermediate. Loss of a H-atom from the nitrogen forms the cis- or trans-

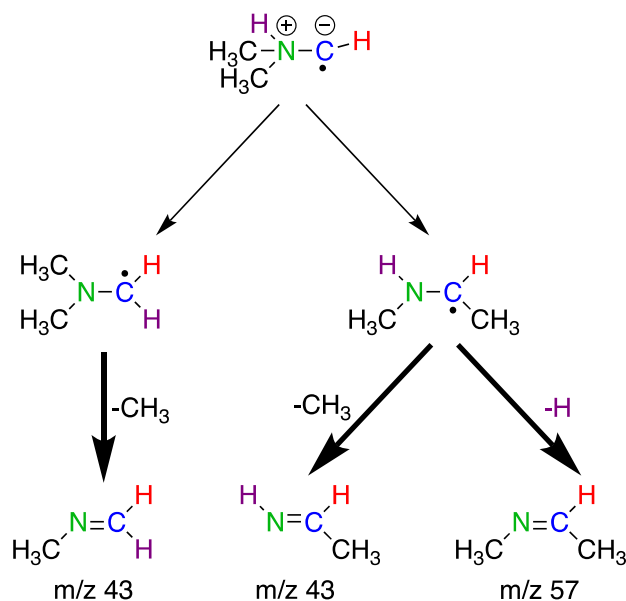
1  
2  
3 methylimine isomers. It is possible that such a mechanism become more favorable as the  
4 number of methyl groups on the reactant amine increases. Further calculations at a higher level  
5 of theory are required in order to discriminate between the direct insertion and dative  
6 intermediate mechanisms for this reaction.  
7  
8  
9  
10  
11  
12



18  
19  
20  
21  
22  
23  
24  
25  
26  
27  
28  
29  
30  
31  
32  
33  
34  
35  
36  
37  
38  
39  
40  
41  
42  
43  
44  
45  
46  
47  
48  
49  
50  
51  
52  
53  
54  
55  
56  
57  
58  
59  
60

Scheme 3

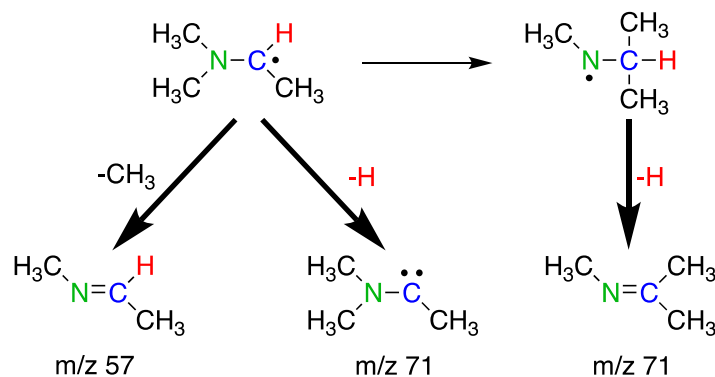
The CH + (CH<sub>3</sub>)<sub>2</sub>NH reaction may be discussed using a similar dative mechanism as those described for the CH + NH<sub>3</sub> and CH + CH<sub>3</sub>NH<sub>2</sub> reactions. As for the reaction of CH with MA, the product detection study does not allow differentiating between a direct N–H/N–C insertion and an addition/isomerization entrance channel. The non-detection of the reactive (CH<sub>3</sub>)<sub>2</sub>N–CH and CH<sub>3</sub>HN–CH amino carbenes suggests that direct decomposition of the (CH<sub>3</sub>)<sub>2</sub>HN–CH dative adduct through H- or CH<sub>3</sub>-loss is not a competitive channel. Scheme 4 shows the proposed mechanism based on the isomerization of a datively bond intermediate to form imine products. Bold arrows correspond to observed channels. Pathways to amino carbene compounds are not shown.



## Scheme 4

The initial  $(\text{CH}_3)_2\text{HN}-\text{CH}$  dative intermediate may isomerize to  $(\text{CH}_3)_2\text{N}-\text{CH}_2$  or  $\text{CH}_3\text{HN}-\text{CHCH}_3$  through H- or  $\text{CH}_3$ -transfers, respectively. The detection of  $\text{CH}_3\text{N}=\text{CH}_2$  and  $\text{HN}=\text{CHCH}_3$  may be explained by loss of a methyl group on the nitrogen atom from the H-transfer and the  $\text{CH}_3$ -transfer isomers. Loss of a H atom from the  $\text{CH}_3\text{HN}-\text{CHCH}_3$  isomer leads to the observed  $\text{CH}_3\text{N}=\text{CHCH}_3$  product at  $m/z$  57. The  $\text{CH}_3\text{HN}-\text{CHCH}_3$  intermediate may also be formed through a more direct C-H insertion mechanism as proposed in scheme 3 for the methyl substituted amine. The fit to the photoionization spectrum in Figure 8 suggests the detection of the  $\text{HN}=\text{C}(\text{CH}_3)_2$  isomer. Its formation through the formation of the dative intermediate would require the transfer of two methyl groups from the nitrogen atom to the carbon atom to give the  $\text{HN}-\text{CH}(\text{CH}_3)_2$  intermediate or one methyl group through a C-H or N-C insertion mechanism.

The main observed H- and  $\text{CH}_3$ -loss products from the  $\text{CH} + (\text{CH}_3)_3\text{N}$  reaction are  $\text{CH}_3\text{N}=\text{CH}_2$  and  $\text{HN}=\text{CHCH}_3$  at  $m/z$  43 and  $\text{CH}_3\text{N}=\text{C}(\text{CH}_3)_2$  at  $m/z$  71. Isomers at  $m/z$  57 are also detected but are a minor pathway with an overall ion signal representing only 10% of the identified reaction products. Scheme 5 displays the possible reaction pathways following isomerization of the  $(\text{CH}_3)_3\text{N}-\text{CH}$  dative adduct by methyl transfer or isomerization of the C-H insertion adduct by H-transfer. Bold arrows correspond to observed channels. The minor dimethylimine channel detected at  $m/z$  57 may be formed by methyl loss from the  $(\text{CH}_3)_2\text{N}-\text{CHCH}_3$  intermediate to give  $\text{CH}_3\text{N}-\text{CHCH}_3$ . Formation of  $\text{HN}=\text{C}(\text{CH}_3)_2$  would require a methyl group transfer and a H-transfer, which is unlikely.



Scheme 5

In scheme 5, formation of the  $\text{CH}_3\text{N}=\text{C}(\text{CH}_3)_2$  isomer at  $m/z\ 71$  requires the transfer of a  $\text{CH}_3$  group from the  $(\text{CH}_3)_2\text{N}-\text{CHCH}_3$  intermediate to form a  $\text{CH}_3\text{N}-\text{CH}(\text{CH}_3)_2$  intermediate followed by H-loss. This mechanism is similar to the successive two-H-atom transfers predicted by Blitz *et al.*<sup>15</sup> for the  $\text{CH} + \text{NH}_3$  reaction. High-level quantum calculations and RRKM-based master equation calculations would be useful to explore these mechanisms in more detail. Formation of methylimine products by the  $\text{CH} + \text{TMA}$  reaction requires the loss of an ethyl group. Although we do detect methylimines at  $m/z = 43$  in this reaction, the absence of signal from the expected co-product  $\text{C}_2\text{H}_5$  radical ( $\text{IE}=8.12\ \text{eV}$ )<sup>65</sup> in Figure 9 is puzzling.

## 5.2 Relevance for combustion chemistry

Prediction of  $\text{NO}_x$  formation from combustion processes is a very active subject of research, especially due to the increasing use of fuels derived from biogenic sources (*e.g.*, biomass, agricultural wastes).<sup>70-74</sup> Biomass combustion could contribute to nitrogen conversion through the formation of nitrogenized intermediates such as HCN. Their formation may depend on the fuel structure. Accordingly, several studies have focused on flames burning nitrogenized compounds (*e.g.*, ammonia, pyrrole, pyridine).<sup>75-80</sup> The spatial detection of nitrogen containing radicals in laminar flames of DMA, ethylamine,<sup>81</sup> and morpholine<sup>82</sup> suggests that the  $\text{NH}_2$  radical is formed very early in the combustion process and further reacts to form HCN, CN, and NO. The mole fraction of ammonia is also found to be relatively large ( $6 \times 10^{-2}$ ) and is likely

1  
2  
3 to play a role in the formation of nitrogen reactive species and nitrogen containing  
4 hydrocarbons. The reactions of ammonia with other abundant combustion radicals is therefore  
5 likely to affect the formation of  $\text{NH}_2$  radicals and ultimately NO. In the present study, the  
6 abstraction channel  $\text{NH}_2 + \text{CH}_2$  from the  $\text{CH} + \text{NH}_3$  reaction is not detected at the temperature  
7 of the flow (373 K). This product channel is calculated to be endothermic by  $20.9 \text{ kJ mol}^{-1}$   
8 (CCSD(T))<sup>15</sup> and could become accessible at flame temperatures ( $>2000 \text{ K}$ ). The formation of  
9 the thermodynamically favorable  $\text{HN}=\text{CH}_2$  may still remain a dominant pathway. Further  
10 reaction of the detected imine may lead to larger nitrogen containing molecules and contribute  
11 to incorporating nitrogen in large hydrocarbons such as polycyclic nitrogen containing  
12 aromatic hydrocarbons.  
13  
14  
15  
16  
17  
18  
19  
20  
21  
22  
23  
24  
25

26  
27 Imine and methyl substituted imines have been detected during the combustion of  
28 biomass model fuels.<sup>82</sup> As for ammonia, the reaction of methyl substituted amines with the CH  
29 radical may contribute to their formation and to the overall molecular growth scheme in  
30 combustion. Abstraction of a H-atom from the carbon group substituent may become more  
31 likely as the number of C–H bonds increase. The product detection performed in the present  
32 study together with the temperature independent rate coefficient reported by Zabarnick *et al.*<sup>14</sup>  
33 suggest that the addition–elimination mechanism will still play a role even at combustion-  
34 relevant temperatures. The isomer resolved detection of the methyl substituted imines and their  
35 proposed formation mechanisms is likely to improve the quality of the chemical models used  
36 to reproduce their spatial molar fraction in flames.<sup>82</sup>  
37  
38  
39  
40  
41  
42  
43  
44  
45  
46  
47  
48  
49

## 50 VI. CONCLUSION

51  
52 The systematic study of the reaction of the methylidyne radical with ammonia, methyl,  
53 dimethyl, and trimethyl amine provides empirical evidence supporting a general reaction  
54 mechanism for CH reacting with amines. The detection of mainly the imine isomer upon  
55 reaction of CH with ammonia is in agreement with the mechanism proposed by Blitz *et al.*<sup>15</sup>  
56  
57  
58  
59  
60

1  
2  
3 based on high-level calculations and RRKM-based master equation calculations. According to  
4 this mechanism, the insertion of the CH radical onto a N–H bond proceeds by the initial  
5 formation of a dative C–N bond. The donor–acceptor type mechanism is barrierless and is  
6 likely to occur over a wide range of temperatures, including under combustion conditions.  
7  
8  
9

10  
11  
12 Although no theoretical data are available for the CH reaction with methyl substituted  
13 amines, a similar mechanism as that proposed for the reaction with ammonia may be employed  
14 to interpret the products detected for the CH + MA, DMA, and TMA. For each reaction, the  
15 detection of H- and CH<sub>3</sub>-loss products may be explained in part through isomerization of an  
16 initial dative adduct formed by the sharing of the nitrogen lone pair with the carbon atom of  
17 the CH radical. Kinetic traces of the reaction products show no evidence of the formation of  
18 the reactive methyl-substituted amino carbene isomers. The detection of the methylimine with  
19 the methyl group on the carbon atom in the case of the CH + MA reaction suggests that the  
20 transfer of a methyl group could be a competitive pathway, but our calculations show a barrier  
21 well above reactant energy for this process. However, a direct insertion pathway of the CH  
22 radical into a methyl C–H bond may become competitive as the number of methyl group  
23 increases. Our data do not allow differentiating between a dative mechanism and direct  
24 insertion, but provide evidence that the latter should be considered. In the case of the CH +  
25 TMA reaction, direct insertion of the CH radical into a C–H bond would lead to a pathway  
26 involving only one CH<sub>3</sub>-transfer followed by H-loss to explain the formation of the detected  
27 CH<sub>3</sub>N=C(CH<sub>3</sub>)<sub>2</sub> isomer. Methylimine isomers are detected from both the CH + DMA and CH  
28 + TMA reactions. The lack of imine absolute ionization cross section does not allow to quantify  
29 their branching fractions. In the case of the CH + TMA reaction formation of methylimines  
30 should also produce a C<sub>2</sub>H<sub>5</sub> radical, which we do not observe.  
31  
32  
33  
34  
35  
36  
37  
38  
39  
40  
41  
42  
43  
44  
45  
46  
47  
48  
49  
50  
51  
52  
53  
54

55  
56 Overall the dative reaction mechanism proposed by Blitz *et al.*<sup>15</sup> for the CH + NH<sub>3</sub>  
57 reaction as well as Ramasami *et al.*<sup>67</sup> for the CH<sub>2</sub>/CHCl/CHF + CH<sub>3</sub>NH<sub>2</sub> is not sufficient to  
58  
59  
60

1  
2  
3 explain all the detected products and a C–H insertion mechanism is likely to become favorable  
4  
5 for alkyl substituted amines. Although the present studies provide valuable data for the  
6  
7 understanding of the reactivity of amines with the CH radical, further theoretical studies  
8  
9 including RRKM-based master equations on the potential energy surface and experimental  
10  
11 studies of photoionization cross sections are paramount toward the full understanding of the  
12  
13 reaction mechanism, especially about the competition between direct N–C insertion and  
14  
15 formation of an initial dative intermediate.  
16  
17

## 18 19 **ACKNOWLEDGEMENTS**

20  
21  
22 The Rennes team acknowledges support from the Agence Nationale de la Recherche, contract  
23  
24 ANR-11-BS04-024- CRESUSOL-01, the French INSU/CNRS Program “Physique et Chimie  
25  
26 du Milieu Interstellaire” (PCMI), the Institut National de Physique (INPCNRS), the Région  
27  
28 Bretagne and the Université de Rennes 1. S.D.L.P. acknowledges financial support from the  
29  
30 Institut Universitaire de France. FG and KLC acknowledge travel support from the Eberly  
31  
32 College of Art and Sciences and The Bennett Department of Chemistry at West Virginia  
33  
34 University as well as the WVU Research Corporation PSCoR program. We thank Messrs.  
35  
36 Howard Johnsen and Raybel Almeida for technical support of this experiment. D.L.O. and the  
37  
38 instrumentation for this work are supported by the Division of Chemical Sciences,  
39  
40 Geosciences, and Biosciences, the Office of Basic Energy Sciences, the U.S. Department of  
41  
42 Energy. Sandia National Laboratories is a multimission laboratory managed and operated by  
43  
44 National Technology and Engineering Solutions of Sandia, LLC., a wholly owned subsidiary  
45  
46 of Honeywell International, Inc. for the U.S. DOE’s National Nuclear Security Administration  
47  
48 under contract DE-NA0003525. This paper describes objective technical results and analysis.  
49  
50 Any subjective views or opinions that might be expressed in the paper do not necessarily  
51  
52 represent the views of the USDOE or the United States Government. This research used  
53  
54 resources of the Advanced Light Source, a DOE Office of Science User Facility, which is  
55  
56  
57  
58  
59  
60

1  
2  
3 supported by the Direct, Office of Science, Office of Basic Energy Sciences, the U.S.  
4  
5 Department of Energy under contract DE-AC02-05CH11231 at Lawrence Berkeley National  
6  
7 Laboratory.  
8  
9

10  
11 **Supporting Information:** Normalized integrated Franck-Condon factors and photoelectron  
12 spectra of the imines and amino carbene isomers.  
13  
14  
15  
16  
17  
18  
19  
20  
21  
22  
23  
24  
25  
26  
27  
28  
29  
30  
31  
32  
33  
34  
35  
36  
37  
38  
39  
40  
41  
42  
43  
44  
45  
46  
47  
48  
49  
50  
51  
52  
53  
54  
55  
56  
57  
58  
59  
60

## References

- (1) Ge, X.; Wexler, A. S.; Clegg, S. L. Atmospheric amines—Part II. Thermodynamic properties and gas/particle partitioning. *Atmos. Environ.* **2011**, *45*, 561-577.
- (2) Ge, X.; Wexler, A. S.; Clegg, S. L. Atmospheric amines—Part I. A review. *Atmos. Environ.* **2011**, *45*, 524-546.
- (3) Cullis, C. F.; Khokhar, B. A. The inhibiting influence of aliphatic amines on the explosive oxidation of acetaldehyde. *Trans. Faraday Society* **1960**, *56*, 1235-1244.
- (4) Shi, J. C.; Shang, Y. L.; Ye, W.; Zhang, R. T.; Luo, S. N. Shock-tube experiments and chemical kinetic modeling study of CH<sub>4</sub> sensitized by CH<sub>3</sub>NHCH<sub>3</sub>. *Energy & Fuels* **2018**, *32*, 5588-5595.
- (5) Moore, F.; Tipper, C. F. H. The effect of additives on low-temperature hydrocarbon ignition in a flow system. *Combust. Flame* **1972**, *19*, 81-87.
- (6) Lucassen, A.; Zhang, K.; Warkentin, J.; Moshhammer, K.; Glarborg, P.; Marshall, P.; Kohse-Höinghaus, K. Fuel-nitrogen conversion in the combustion of small amines using dimethylamine and ethylamine as biomass-related model fuels. *Combust. Flame* **2012**, *159*, 2254-2279.
- (7) Tipper, C. F. H.; Titchard, A. The effect of additives on the cool flame combustion of n-heptane. *Combust. Flame* **1971**, *16*, 223-232.
- (8) Jones, P. W.; Selby, K.; Tidball, M. J.; Waddington, D. J. Inhibition of gas-phase oxidation reactions by aliphatic amines and related compounds. *Combust. Flame* **1974**, *22*, 209-217.
- (9) Atkinson, R.; Pitts Jr, J. N. Kinetics of the reactions of O (<sup>3</sup>P) atoms with the amines CH<sub>3</sub>NH<sub>2</sub>, C<sub>2</sub>H<sub>5</sub>NH<sub>2</sub>, (CH<sub>3</sub>)<sub>2</sub>NH, and (CH<sub>3</sub>)<sub>3</sub>N over the temperature range 298–440 K. *J. Chem. Phys.* **1978**, *68*, 911-915.

- 1  
2  
3 (10) Slagle, I. R.; Dudich, J. F.; Gutman, D. Direct identification of reactive routes in the  
4 reaction of oxygen atoms with dimethylamine. *Chem. Phys. Lett.* **1979**, *61*, 620-624.  
5  
6  
7 (11) Atkinson, R.; Baulch, D. L.; Cox, R. A.; Crowley, J. N.; Hampson, R. F.; Hynes, R. G.;  
8 Jenkin, M. E.; Rossi, M. J.; Troe, J. Evaluated kinetic and photochemical data for  
9 atmospheric chemistry: Volume I - gas phase reactions of O<sub>x</sub>, HO<sub>x</sub>, NO<sub>x</sub> and SO<sub>x</sub> species.  
10  
11  
12  
13  
14  
15 *Atmos. Chem. Phys.* **2004**, *4*, 1461-1738.  
16  
17 (12) Sims, I. R.; Queffelec, J. L.; Defrance, A.; Rebrionrowe, C.; Travers, D.; Bocherel, P.;  
18 Rowe, B. R.; Smith, I. W. M. Ultralow temperature kinetics of neutral-neutral reactions - The  
19 technique and results for the reactions CN + O<sub>2</sub> down to 13 K and CN+NH<sub>3</sub> down to 25 K. *J.*  
20  
21  
22  
23  
24  
25 *Chem. Phys.* **1994**, *100*, 4229-4241.  
26  
27 (13) Nizamov, B.; Leone, S. R. Rate Coefficients and Kinetic Isotope Effect for the C<sub>2</sub>H  
28 Reactions with NH<sub>3</sub> and ND<sub>3</sub> in the 104– 294 K Temperature Range. *J. Phys. Chem. A* **2004**,  
29  
30  
31  
32 *108*, 3766-3771.  
33 (14) Zabarnick, S.; Fleming, J. W.; Lin, M. C. Kinetics of the methylidyne (CHX<sup>2</sup>PI) radical  
34 reactions with ammonia and methylamines. *Chem. Phys.* **1989**, *132*, 407-411.  
35  
36 (15) Blitz, M. A.; Talbi, D.; Seakins, P. W.; Smith, I. W. M. Rate constants and branching  
37 ratios for the reaction of CH radicals with NH<sub>3</sub>: A combined experimental and theoretical  
38 study. *J. Phys. Chem. A* **2012**, *116*, 5877-5885.  
39  
40  
41  
42 (16) Corchado, J. C.; Espinosa-Garcia, J.; Hu, W.-P.; Rossi, I.; Truhlar, D. G. Dual-level  
43 reaction-path dynamics (the approach to VTST with semiclassical tunneling). Application to  
44 OH+ NH<sub>3</sub>. fwdarw. H<sub>2</sub>O+ NH<sub>2</sub>. *J. Phys. Chem.* **1995**, *99*, 687-694.  
45  
46  
47  
48  
49 (17) Meads, R. F.; Maclagan, R. G.; Phillips, L. F. Kinetics, energetics, and dynamics of the  
50 reactions of cyanogen with ammonia and ammonia-d<sub>3</sub>. *J. Phys. Chem.* **1993**, *97*, 3257-3265.  
51  
52  
53  
54  
55  
56  
57  
58  
59  
60



- 1  
2  
3 (26) Vereecken, L.; Pierloot, K.; Peeters, J. B3LYP-DFT characterization of the potential  
4 energy surface of the CH ( $X^2\Pi$ ) + C<sub>2</sub>H<sub>2</sub> reaction. *J. Chem. Phys.* **1998**, *108*, 1068-1080.  
5  
6  
7 (27) Vereecken, L.; Peeters, J. Detailed microvariational RRKM master equation analysis of  
8 the product distribution of the C<sub>2</sub>H<sub>2</sub> + CH ( $X^2\Pi$ ) reaction over extended temperature and  
9 pressure ranges. *J. Phys. Chem. A* **1999**, *103*, 5523-5533.  
10  
11  
12 (28) Goulay, F.; Trevitt, A. J.; Meloni, G.; Selby, T. M.; Osborn, D. L.; Taatjes, C. A.;  
13 Vereecken, L.; Leone, S. R. Cyclic versus linear isomers produced by reaction of the  
14 methylidyne radical (CH) with small unsaturated hydrocarbons. *J. Am. Chem. Soc.* **2009**, *131*,  
15 993-1005.  
16  
17  
18 (29) Fenimore, C. P. Formation of nitric oxide in premixed hydrocarbon flames. *Proc.*  
19 *Comb. Instit.* **1971**, *13*, 373-380.  
20  
21  
22 (30) Miller, J. A.; Bowman, C. T. Mechanism and modeling of nitrogen chemistry in  
23 combustion. *Prog. Energy Combust. Sci.* **1989**, *15*, 287-338.  
24  
25  
26 (31) Becker, K. H.; Engelhardt, B.; Geiger, H.; Kurtenbach, R.; Schrey, G.; Wiesen, P.  
27 Temperature dependence of the CH + N<sub>2</sub> reaction at low total pressure. *Chem. Phys. Lett.*  
28 **1992**, *195*, 322-328.  
29  
30  
31 (32) Becker, K. H.; Engelhardt, B.; Geiger, H.; Kurtenbach, R.; Weisen, P. Temperature  
32 dependence of the reactions of CH radicals with NO, NH<sub>3</sub> and N<sub>2</sub>O in the range 200-1300 K.  
33 *Chem. Phys. Lett.* **1993**, *210*, 135-140.  
34  
35  
36 (33) Becker, K. H.; Engelhardt, B.; Geiger, H.; Kurtenbach, R.; Wiesen, P. Temperature  
37 dependence of the reactions of CH radicals with NO, NH<sub>3</sub> and N<sub>2</sub>O in the range 200-1300-K.  
38 *Chem. Phys. Lett.* **1993**, *210*, 135-140.  
39  
40  
41 (34) Geiger, H.; Wiesen, P.; Becker, K. H. A product study of the reaction of CH radicals  
42 with nitric oxide at 298 K. *Phys. Chem. Chem. Phys.* **1999**, *1*, 5601-5606.  
43  
44  
45  
46  
47  
48  
49  
50  
51  
52  
53  
54  
55  
56  
57  
58  
59  
60

- 1  
2  
3 (35) Cui, Q.; Morokuma, K.; Bowman, J. M.; Klippenstein, S. J. The spin-forbidden reaction  
4  
5 CH ( $^2\Pi$ ) + N<sub>2</sub> → HCN + N ( $^4S$ ) revisited. II. Nonadiabatic transition state theory and  
6  
7 application. *J. Chem. Phys.* **1999**, *110*, 9469-9482.  
8  
9  
10 (36) Moskaleva, L. V.; Lin, M. C. The spin-conserved reaction CH + N<sub>2</sub> → H + NCN: A  
11  
12 major pathway to prompt NO studied by quantum/statistical theory calculations and kinetic  
13  
14 modeling of rate constant. *Proc. Comb. Instit.* **2000**, *28*, 2393-2401.  
15  
16  
17 (37) Berman, M. R.; Tsuchiya, T.; Gregušová, A.; Perera, S. A.; Bartlett, R. J. HNNC radical  
18  
19 and its role in the CH + N<sub>2</sub> reaction. *J. Phys. Chem. A* **2007**, *111*, 6894-6899.  
20  
21  
22 (38) Goos, E.; Sickfeld, C.; Mauß, F.; Seidel, L.; Ruscic, B.; Burcat, A.; Zeuch, T. Prompt  
23  
24 NO formation in flames: The influence of NCN thermochemistry. *Proc. Comb. Instit.* **2013**,  
25  
26 *34*, 657-666.  
27  
28  
29 (39) Bocherel, P.; Herbert, L. B.; Rowe, B. R.; Sims, I. R.; Smith, I. W.; Travers, D.  
30  
31 Ultralow-temperature kinetics of CH ( $X^2\Pi$ ) reactions: Rate coefficients for reactions with O<sub>2</sub>  
32  
33 and NO (T = 13–708 K), and with NH<sub>3</sub> (T = 23–295 K). *J. Phys. Chem.* **1996**, *100*, 3063-  
34  
35 3069.  
36  
37  
38 (40) Trevitt, A. J.; Goulay, F. Insights into gas-phase reaction mechanisms of small carbon  
39  
40 radicals using isomer-resolved product detection. *Phys. Chem. Chem. Phys.* **2016**, *18*, 5867-  
41  
42 5882.  
43  
44  
45 (41) Osborn, D. L.; Zou, P.; Johnsen, H.; Hayden, C. C.; Taatjes, C. A.; Knyazev, V. D.;  
46  
47 North, S. W.; Peterka, D. S.; Ahmed, M.; Leone, S. R. The multiplexed chemical kinetic  
48  
49 photoionization mass spectrometer: A new approach to isomer-resolved chemical kinetics.  
50  
51 *Rev. Sci. Instrum.* **2008**, *79*, 104103: 1-10.  
52  
53  
54 (42) Taatjes, C. A.; Hansen, N.; Osborn, D. L.; Kohse-Höinghaus, K.; Cool, T. A.;  
55  
56 Westmoreland, P. R. “Imaging” combustion chemistry via multiplexed synchrotron-  
57  
58 photoionization mass spectrometry. *Phys. Chem. Chem. Phys.* **2008**, *10*, 20-34.  
59  
60

- 1  
2  
3 (43) Goulay, F.; Trevitt, A. J.; Savee, J. D.; Bouwman, J.; Osborn, D. L.; Taatjes, C. A.;  
4  
5 Wilson, K. R.; Leone, S. R. Product detection of the CH radical reaction with acetaldehyde.  
6  
7 *J. Phys. Chem. A* **2012**, *116*, 6091-6106.  
8  
9  
10 (44) Zou, P.; Shu, J.; Sears, T. J.; Hall, G. E.; North, S. W. Photodissociation of bromoform  
11  
12 at 248 nm: Single and multiphoton processes. *J. Phys. Chem. A* **2004**, *108*, 1482-1488.  
13  
14 (45) Romanzin, C.; Boye-Peronne, S.; Gauyacq, D.; Benilan, Y.; Gazeau, M. C.; Douin, S.  
15  
16 CH radical production from 248 nm photolysis or discharge-jet dissociation of CHBr<sub>3</sub> probed  
17  
18 by cavity ring-down absorption spectroscopy. *J. Chem. Phys.* **2006**, *125*, 114312: 1-9.  
19  
20 (46) Bourgalais, J.; Spencer, M.; Osborn, D. L.; Goulay, F.; Le Picard, S. D. Reactions of  
21  
22 atomic carbon with butene isomers: Implications for molecular growth in carbon-rich  
23  
24 environments. *J. Phys. Chem. A* **2016**, *120*, 9138-9150.  
25  
26  
27 (47) Capron, M.; Bourgalais, J.; Kailasanathan, R. K. A.; Osborn, D. L.; Le Picard, S. D.;  
28  
29 Goulay, F. Flow tube studies of the C (<sup>3</sup>P) reactions with ethylene and propylene. *Phys.*  
30  
31 *Chem. Chem. Phys.* **2015**, *17*, 23833-23846.  
32  
33  
34 (48) Montgomery, J. A.; Frisch, M. J.; Ochterski, J. W.; Petersson, G. A. A complete basis  
35  
36 set model chemistry. VI. Use of density functional geometries and frequencies. *J. Chem.*  
37  
38 *Phys.* **1999**, *110*, 2822-2827.  
39  
40  
41 (49) Montgomery, J. A.; Frisch, M. J.; Ochterski, J. W.; Petersson, G. A. A complete basis  
42  
43 set model chemistry. VII. Use of the minimum population localization method. *J. Chem.*  
44  
45 *Phys.* **2000**, *112*, 6532-6542.  
46  
47  
48 (50) Barone, V.; Bloino, J.; Biczysko, M.; Santoro, F. Fully integrated approach to compute  
49  
50 vibrationally resolved optical spectra: from small molecules to macrosystems. *J. Chem. Theo.*  
51  
52 *Comput.* **2009**, *5*, 540-554.  
53  
54  
55  
56  
57  
58  
59  
60

- 1  
2  
3 (51) Goulay, F.; Rebrion-Rowe, C.; Biennier, L.; Le Picard, S. D.; Canosa, A.; Rowe, B. R.  
4  
5 Reaction of anthracene with CH radicals: An experimental study of the kinetics between 58  
6  
7 and 470 K. *J. Phys. Chem. A* **2006**, *110*, 3132-3137.  
8  
9  
10 (52) Herbert, L. B.; Sims, I. R.; Smith, I. W. M.; Stewart, D. W. A.; Symonds, A.; Canosa,  
11  
12 A.; Rowe, B. R. Rate constants for the relaxation of CH(X(2)pi,nu=1) by CO and N-2 at  
13  
14 temperatures from 23 to 584 K. *J. Phys. Chem.* **1996**, *100*, 14928-14935.  
15  
16  
17 (53) Brownsword, R. A.; Herbert, L. B.; Smith, I. W. M.; Stewart, D. W. A. Pressure and  
18  
19 temperature dependence of the rate constants for the association reactions of CH radicals with  
20  
21 CO and N-2 between 202 and 584 K. *J. Chem. Soc., Faraday* **1996**, *92*, 1087-1094.  
22  
23  
24 (54) Ruzsicska, B. P.; Jodhan, A.; Choi, H. K. J.; Strausz, O. P.; Bell, T. N. Chemistry of  
25  
26 carbynes: reaction of CF, CCl, and CBr with alkenes. *J. Am. Chem. Soc.* **1983**, *105*, 2489-  
27  
28 2490.  
29  
30  
31 (55) James, F. C.; Ruzsicska, B.; McDaniel, R. S.; Dickson, R.; Strausz, O. P.; Bell, T. N.  
32  
33 Rate constants for the reaction of the bromomethyne radical with alkynes. *Chem. Phys. Lett.*  
34  
35 **1977**, *45*, 449-453.  
36  
37  
38 (56) McDaniel, R. S.; Dickson, R.; James, F. C.; Strausz, O. P.; Bell, T. N. Rate parameters  
39  
40 for the reactions of the bromomethyne radical. *Chem. Phys. Lett.* **1976**, *43*, 130-134.  
41  
42  
43 (57) Daugey, N.; Caubet, P.; Retail, B.; Costes, M.; Bergeat, A.; Dorthe, G. Kinetic  
44  
45 measurements on methylidyne radical reactions with several hydrocarbons at low  
46  
47 temperatures. *Phys. Chem. Chem. Phys.* **2005**, *7*, 2921-2927.  
48  
49  
50 (58) Canosa, A.; Sims, I. R.; Travers, D.; Smith, I. W. M.; Rowe, B. R. Reactions of the  
51  
52 methylidene radical with CH<sub>4</sub>, C<sub>2</sub>H<sub>2</sub>, C<sub>2</sub>H<sub>4</sub>, C<sub>2</sub>H<sub>6</sub>, and but-1-ene studied between 23 and 295K  
53  
54 with a CRESU apparatus. *Astron. Astrophys.* **1997**, *323*, 644-651.  
55  
56  
57  
58  
59  
60

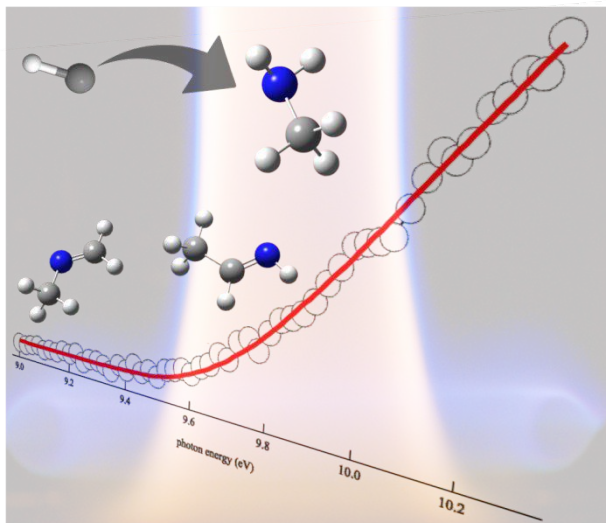
- 1  
2  
3 (59) Goulay, F.; Derakhshan, A.; Maher, E.; Trevitt, A. J.; Savee, J. D.; Scheer, A. M.;  
4  
5 Osborn, D. L.; Taatjes, C. A. Formation of dimethylketene and methacrolein by reaction of  
6  
7 the CH radical with acetone. *Phys. Chem. Chem. Phys.* **2013**, *15*, 4049-58.  
8  
9  
10 (60) Cheng, B.-M.; Lu, H.-C.; Chen, H.-K.; Bahou, M.; Lee, Y.-P.; Mebel, A. M.; Lee, L.  
11  
12 C.; Liang, M.-C.; Yung, Y. L. Absorption cross sections of NH<sub>3</sub>, NH<sub>2</sub>D, NHD<sub>2</sub>, and ND<sub>3</sub> in  
13  
14 the spectral range 140-220 nm and implications for planetary isotopic fractionation.  
15  
16 *Astrophys. J.* **2006**, *647*, 1535-1542.  
17  
18  
19 (61) Hubin-Franskin, M.-J.; Delwiche, J.; Giuliani, A.; Ska, M.-P.; Motte-Tollet, F.; Walker,  
20  
21 I. C.; Mason, N. J.; Gingell, J. M.; Jones, N. C. Electronic excitation and optical cross  
22  
23 sections of methylamine and ethylamine in the UV–VUV spectral region. *J. Chem. Phys.*  
24  
25 **2002**, *116*, 9261-9268.  
26  
27  
28 (62) Halpern, A. M.; Ondrechen, M. J.; Ziegler, L. D. Analysis of the absorption and  
29  
30 fluorescence spectra of trimethylamine - Determination of the A-X origin and the ground-  
31  
32 state inversion barrier. *J. Am. Chem. Soc.* **1986**, *108*, 3907-3912.  
33  
34  
35 (63) Bock, H.; Dammel, R. Methanimines RR'C=NR" - Preparation and photoelectron  
36  
37 spectra. *Chemische Berichte-Recueil* **1987**, *120*, 1961-1970.  
38  
39  
40 (64) Bobeldijk, M.; van der Zande, W. J.; Kistemaker, P. G. Simple models for the  
41  
42 calculation of photoionization and electron impact ionization cross section of polyatomic  
43  
44 molecules. *Chem. Phys.* **1994**, *179*, 125-130.  
45  
46  
47 (65) NIST, 2005, Standard Reference Database Number 69, NIST Chemistry WebBook,  
48  
49 National Institute of Standards and Technology, Gaithersburg MD, 20899  
50  
51 (<http://webbook.nist.gov>).  
52  
53  
54 (66) Savee, J. D.; Welz, O.; Taatjes, C. A.; Osborn, D. L. New mechanistic insights to the  
55  
56 O(<sup>3</sup>P) + propene reaction from multiplexed photoionization mass spectrometry. *Phys. Chem.*  
57  
58 *Chem. Phys.* **2012**, *14*, 10410-10423.  
59  
60

- 1  
2  
3 (67) Ramasami, K.; Ramalingam, M.; Venuvanalingam, P. Singlet methylene and  
4 halocarbenes insertions into polar N-H bonds of amines *J. Theo. Comput. Chem.* **2009**, *8*,  
5 1143-1153.  
6  
7  
8  
9  
10 (68) Simmie, J. M.; Somers, K. P. Benchmarking compound methods (CBS-QB3, CBS-  
11 APNO, G3, G4, W1BD) against the active thermochemical tables: A Litmus test for cost-  
12 effective molecular formation enthalpies. *J. Phys. Chem. A* **2015**, *119*, 7235-7246.  
13  
14  
15 (69) Gilbert, T. M. Tests of the MP2 model and various DFT models in predicting the  
16 structures and B-N bond dissociation energies of amine-boranes (X<sub>3</sub>C)(m)H<sub>3</sub>-mB-  
17 H(CH<sub>3</sub>)(n)H<sub>3</sub>-n (X = H, F; m=0-3; n=0-3): Poor performance of the B3LYP approach for  
18 dative B-N bonds. *J. Phys. Chem. A* **2004**, *108*, 2550-2554.  
19  
20  
21  
22  
23  
24  
25  
26 (70) Demirbas, A. Potential applications of renewable energy sources, biomass combustion  
27 problems in boiler power systems and combustion related environmental issues. *Prog.*  
28 *Energy Combust. Sci.* **2005**, *31*, 171-192.  
29  
30  
31  
32  
33 (71) Kohse-Höinghaus, K.; Oßwald, P.; Cool, T. A.; Kasper, T.; Hansen, N.; Qi, F.;  
34 Westbrook, C. K.; Westmoreland, P. R. Biofuel combustion chemistry: From ethanol to  
35 biodiesel. *Angew. Chem. Int. Ed.* **2010**, *49*, 3572-3597.  
36  
37  
38  
39  
40 (72) Zhang, Y.; Zhang, J.; Sheng, C.; Liu, Y.; Zhao, L.; Ding, Q. Quantitative analysis of  
41 NO<sub>x</sub> reduction in Oxy-coal combustion. *Energy & Fuels* **2011**, *25*, 1146-1152.  
42  
43  
44 (73) Mendiara, T.; Glarborg, P. Ammonia chemistry in oxy-fuel combustion of methane.  
45 *Combust. Flame* **2009**, *156*, 1937-1949.  
46  
47  
48  
49 (74) Darvell, L. I.; Jones, J. M.; Gudka, B.; Baxter, X. C.; Saddawi, A.; Williams, A.;  
50 Malmgren, A. Combustion properties of some power station biomass fuels. *Fuel* **2010**, *89*,  
51 2881-2890.  
52  
53  
54  
55  
56  
57  
58  
59  
60

- 1  
2  
3 (75) Tian, Z.; Li, Y.; Zhang, L.; Glarborg, P.; Qi, F. An experimental and kinetic modeling  
4 study of premixed NH<sub>3</sub>/CH<sub>4</sub>/O<sub>2</sub>/Ar flames at low pressure. *Combust. Flame* **2009**, *156*, 1413-  
5 1426.  
6  
7  
8  
9  
10 (76) Tian, Z.; Li, Y.; Zhang, T.; Zhu, A.; Cui, Z.; Qi, F. An experimental study of low-  
11 pressure premixed pyrrole/oxygen/argon flames with tunable synchrotron photoionization.  
12 *Combust. Flame* **2007**, *151*, 347-365.  
13  
14  
15 (77) Tian, Z.; Li, Y.; Zhang, T.; Zhu, A.; Qi, F. Identification of combustion intermediates in  
16 low-pressure premixed pyridine/oxygen/argon flames. *J. Phys. Chem. A* **2008**, *112*, 13549-  
17 13555.  
18  
19  
20 (78) Wang, Z.; Lucassen, A.; Zhang, L.; Yang, J.; Kohse-Höinghaus, K.; Qi, F.  
21 Experimental and theoretical studies on decomposition of pyrrolidine. *Proc. Comb. Instit.*  
22 **2011**, *33*, 415-423.  
23  
24 (79) Duynslaegher, C.; Jeanmart, H.; Vandooren, J. Flame structure studies of premixed  
25 ammonia/hydrogen/oxygen/argon flames: Experimental and numerical investigation. *Proc.*  
26 *Comb. Instit.* **2009**, *32*, 1277-1284.  
27  
28  
29 (80) Zhang, K.; Li, Y.; Yuan, T.; Cai, J.; Glarborg, P.; Qi, F. An experimental and kinetic  
30 modeling study of premixed nitromethane flames at low pressure. *Proc. Comb. Instit.* **2011**,  
31 *33*, 407-414.  
32  
33  
34 (81) Nau, P.; Seipel, A.; Lucassen, A.; Brockhinke, A.; Kohse-Höinghaus, K. Intermediate  
35 species detection in a morpholine flame: contributions to fuel-bound nitrogen conversion  
36 from a model biofuel. *Exp. Fluids* **2010**, *49*, 761-773.  
37  
38  
39 (82) Lucassen, A.; Labbe, N.; Westmoreland, P. R.; Kohse-Hoinghaus, K. Combustion  
40 chemistry and fuel-nitrogen conversion in a laminar premixed flame of morpholine as a  
41 model biofuel. *Combust. Flame* **2011**, *158*, 1647-1666.  
42  
43  
44  
45  
46  
47  
48  
49  
50  
51  
52  
53  
54  
55  
56  
57  
58  
59  
60

1  
2  
3  
4  
5  
6  
7  
8  
9  
10  
11  
12  
13  
14  
15  
16  
17  
18  
19  
20  
21  
22  
23  
24  
25  
26  
27  
28  
29  
30  
31  
32  
33  
34  
35  
36  
37  
38  
39  
40  
41  
42  
43  
44  
45  
46  
47  
48  
49  
50  
51  
52  
53  
54  
55  
56  
57  
58  
59  
60

TOC



1  
2  
3  
4  
5  
6  
7  
8  
9  
10  
11  
12  
13  
14  
15  
16  
17  
18  
19  
20  
21  
22  
23  
24  
25  
26  
27  
28  
29  
30  
31  
32  
33  
34  
35  
36  
37  
38  
39  
40  
41  
42  
43  
44  
45  
46  
47  
48  
49  
50  
51  
52  
53  
54  
55  
56  
57  
58  
59  
60